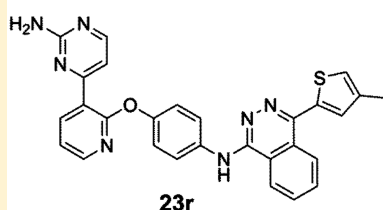


Discovery of *N*-(4-(3-(2-Aminopyrimidin-4-yl)pyridin-2-yloxy)phenyl)-4-(4-methylthiophen-2-yl)phthalazin-1-amine (AMG 900), A Highly Selective, Orally Bioavailable Inhibitor of Aurora Kinases with Activity against Multidrug-Resistant Cancer Cell Lines

Stephanie Geuns-Meyer,^{*,†} Victor J. Cee,[†] Holly L. Deak,[†] Bingfan Du,^{†,#} Brian L. Hodous,^{†,∇} Hanh Nho Nguyen,^{†,○} Philip R. Olivieri,[†] Laurie B. Schenkel,[†] Karina R. Vaida,[†] Paul Andrews,^{||} Annette Bak,^{‡,@} Xuhai Be,[§] Pedro J. Beltran,[⊥] Tammy L. Bush,^{⊥,+} Mary K. Chaves,[‡] Grace Chung,[⊥] Yang Dai,^{§,||} Patrick Eden,[⊥] Kelly Hanestad,[⊥] Liyue Huang,[§] Min-Hwa Jasmine Lin,[§] Jin Tang,^{||} Beth Ziegler,^{⊥,◇} Robert Radinsky,^{⊥,+} Richard Kendall,[⊥] Vinod F. Patel,^{†,⊗} and Marc Payton[⊥]

[†]Departments of Medicinal Chemistry, [‡]Pharmaceutical Research and Development, [§]Pharmacokinetics and Drug Metabolism, ^{||}Molecular Structure, and [⊥]Oncology Research, Amgen Inc., 360 Binney Street, Cambridge, Massachusetts 02142, United States, and Amgen Inc., One Amgen Center Drive, Thousand Oaks, California 91320, United States

S Supporting Information



Cell Line	EC ₅₀ (nM)
CAL51 (Non-MDR)	2
MES-SA Dx5 (MDR)	1
HCT15 (MDR)	2
SNU449 (MDR)	2
769P (MDR)	2

ABSTRACT: Efforts to improve upon the physical properties and metabolic stability of Aurora kinase inhibitor **14a** revealed that potency against multidrug-resistant cell lines was compromised by increased polarity. Despite its high in vitro metabolic intrinsic clearance, **23r** (AMG 900) showed acceptable pharmacokinetic properties and robust pharmacodynamic activity. Projecting from in vitro data to in vivo target coverage was not practical due to disjunctions between enzyme and cell data, complex and apparently contradictory indicators of binding kinetics, and unmeasurable free fraction in plasma. In contrast, it was straightforward to relate pharmacokinetics to pharmacodynamics and efficacy by following the time above a threshold concentration. On the basis of its oral route of administration, a selectivity profile that favors Aurora-driven pharmacology and its activity against multidrug-resistant cell lines, **23r** was identified as a potential best-in-class Aurora kinase inhibitor. In phase 1 dose expansion studies with G-CSF support, **23r** has shown promising single agent activity.

INTRODUCTION

The serine/threonine Aurora kinases A and B (AurA and AurB) play essential and distinct roles in mitosis.¹ Aurora kinases have been implicated in tumorigenesis, with their overexpression levels correlating to clinical staging of cancers and poor prognosis. Thus, these mitotic kinases have been the subject of much interest as targets for anticancer therapy, and many Aurora kinase inhibitors (AKIs) have entered clinical trials.²

AurA is involved in centrosome maturation and the development of bipolar spindles.³ Inhibition of AurA results in abnormal spindles, increased G₂/M cells, delay in mitotic progression, and an increased degree of aneuploidy. AurB activity is necessary for maintaining the spindle assembly checkpoint (SAC), ensuring proper chromosome alignment and segregation, and enabling cytokinesis.⁴ Inhibition of AurB leads to abrogation of the SAC, thereby inducing cells to exit mitosis without dividing. This aborted cytokinesis is a unique

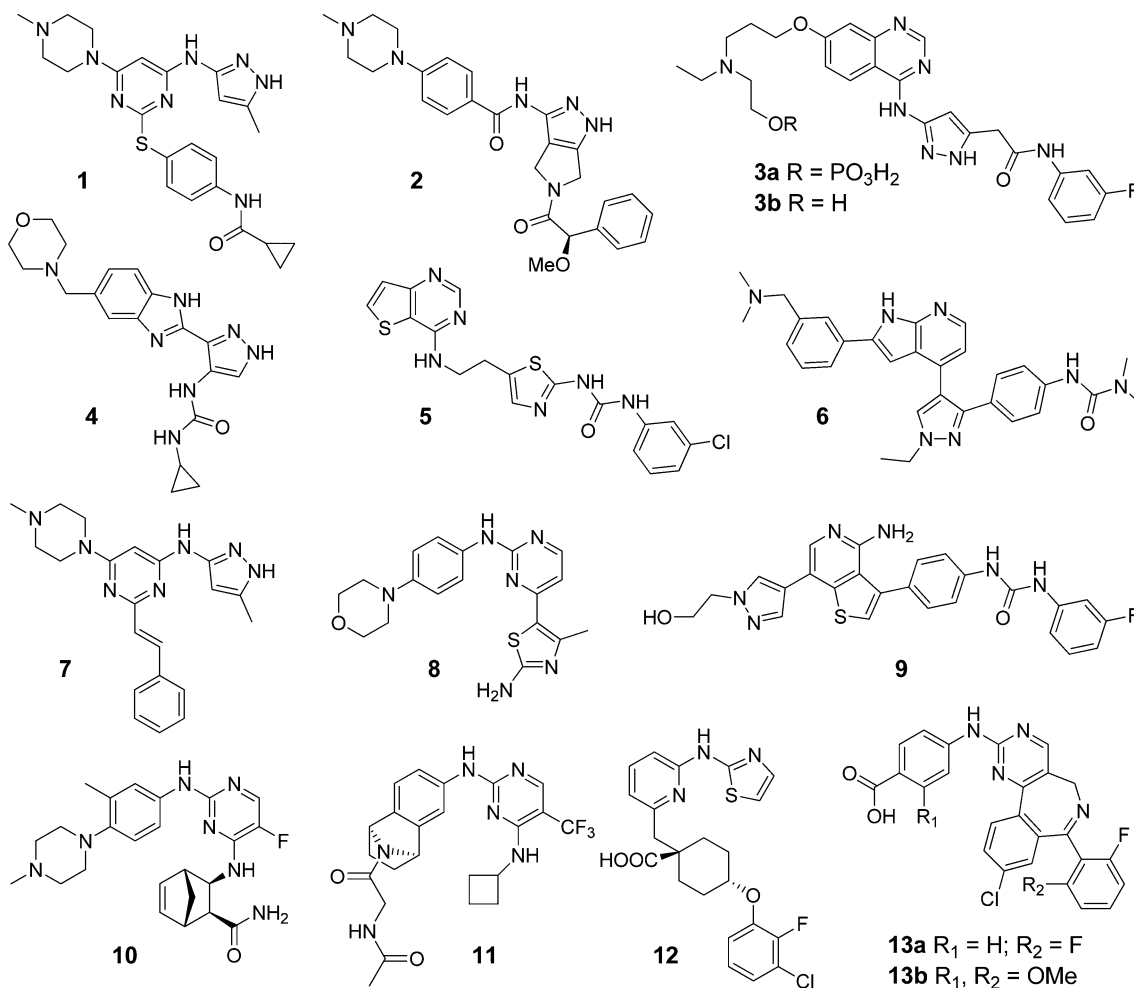
mechanism of blocking mitotic progression relative to other antimitotic mechanisms, including AurA inhibition. In cancer cells, inhibition of AurB can induce apoptosis at the resulting 4N G₁ stage; alternatively, cells may continue to progress through successive cell cycles without division, resulting in a lethal accumulation of DNA. Interestingly, abrogation of the SAC by inhibition of AurB overrides the phenotype induced by inhibition of AurA by itself so that the AurB inhibitory phenotype is dominant with an inhibitor of both kinases.⁵

We have previously described the discovery of a series of pyridinyl-pyrimidine phthalazine AKIs with an AurB inhibitory phenotype, exemplified by the highly selective, orally bioavailable compounds **14a** and **14b** (Table 2).⁶ Our target profile for the clinical candidate that would evolve from this

Received: February 1, 2015

Published: May 13, 2015

Table 1. Aurora Kinase Inhibitors with Known Structures That Have Entered Clinical Trials



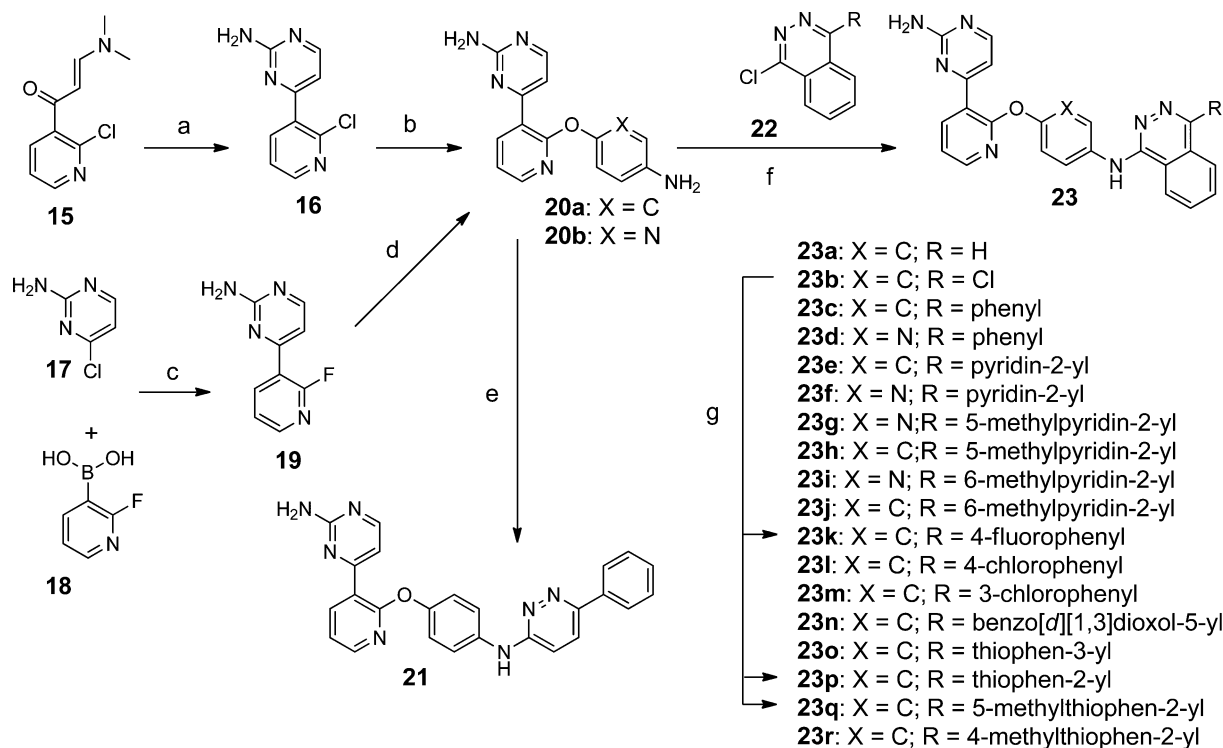
ID, compd name	AK ^a	AK cell assay ^b	(nM)	most potently inhibited non-AKs (nM) ^c [total kinases in panel]	admin route
1 (MK-0457/VX-680/tozasertib) ⁷	A/B	MDA-MB-231 p-HH3 ¹²	43	FLT3 (6), PLK4 (9), ABL (13), MLCK (15), RET (28); [317] ¹⁶	IV
2 (PHA-739358/danuseritib) ⁸	A/B	MDA-MB-231 p-HH3 ¹²	49	ABL (25), RET (31), TrkA (31), FGFR1 (47); [35] ¹⁷	IV
3a (AZD1152/barasertib) ^{d,9}	B	MDA-MB-231 p-HH3 ¹²	16	FLT3 (8), cKIT (17), PDGFRA (38), PDGFRB (41), RET (80); [317] ¹⁶	IV
4 (AT9283) ¹⁸	A/B	HCT-116 DNA ploidy	~30	JAK2 (1), JAK3 (1) Abl (T315I) (4), 9 others ≤10 nM; [230]	IV
5 (SNS-314) ¹⁹	A/B	HCT-116 DNA ploidy ²⁰	9	TrkB (5), TrkA (12), FLT4 (14), Fms (15), DDR2 (82), Axl (84); [219]	IV
6 (GSK1070916) ²¹	B	HCT-116 p-HH3 ²²	20	FLT1 (42), TIE2 (59), SIK (70), FLT4 (74), FGFR (78); [328] ²²	IV
7 (ENMD-2076) ²³	A	HCT-116 p-AurA	130	FLT3 (2), RET (10), FLT4 (16), SRC (20), TrkA (24), Fms (25); [100]	PO
8 (CYC116) ²⁴	A/B	A549 p-HH3	480	VEGFR2 (44), FLT3 (44), CDK2 (390); [23]	PO
9 (ABT-348) ²⁵	A/B	HCT-116 p-HH3	21	VEGFR1 (1), FLT3 (1), VEGFR2 (2), CSF-1R (3), PDGFR-α (11); [128]	PO
10 (AS703569/R763) ²⁶	A/B	A549 p-HH3	14	cell-based assays: VEGFR2 (11), FLT3 (27), AMPK (201); [10]	PO
11 (PF-03814735) ²⁷	A/B	MDA-MB-231 p-HH3	~50	FLT1 (10), FAK (22), TrkA (30), 17 others ≥90% inh@100 nM; [220]	PO
12 (MK-5108) ²⁸	A	HeLa S3 ↑p-HH3+ cells	<1000	TrkA (2), ABL (8), FLT4 (12), TrkB (13), VEGFR2 (30); [233]	PO
13a (MLN8054) ²⁹	A	HCT-116 p-AurA	34	DRAK2 (8), BLK (68), DRAK1 (190), FGR (220); [317] ¹⁶	PO
13b (MLN8237/alisertib) ³⁰	A	HeLa p-AurA	7	%inh@1 μM: EphA2 (111), FGR (97), CAMK2A (95), EphA4 (94); [220]	PO

^aAK = Aurora kinase family member(s) inhibited (AurA and/or AurB; AurC potency not listed). ^bCell line; substrate or phenotype detected.

^cKinase activities of greatest potency listed in published literature. ^dListed enzyme and cellular potency data is for 3b, the parent of prodrug 3a.

class of leads was framed by three AurB phenotype inhibitors in Table 1 that were undergoing phase 1 clinical trials at the time: 1 (MK-0457),⁷ 2 (PHA-739358),⁸ and 3a (AZD1152).⁹ Given the increasingly crowded clinical arena, a compound developed from 14a/b would need to possess potential advantages over known clinical compounds or be better suited to test important clinical hypotheses about the effects of AK inhibition.

High selectivity against other kinases was a key attribute of the phthalazines we intended to maintain. For example, 14b provided IC₅₀ values <25 nM in AurB enzyme and cellular assays and >58-fold enzyme selectivity against a panel of 19 diverse kinases; 14b showed the strongest non-AK activity against Tie-2 (872 nM) and no significant inhibition of 17 of the other kinases at concentrations up to 25 μM.⁶ Inhibition of off-target kinases may provide anticancer activities through

Scheme 1. Preparation of Substituted Pyridazine and Phthalazine Pyridinyl Pyrimidine AKIs^a

^aReagents and conditions: (a) guanidine-HCl, NaOMe, MeOH, 50 °C, 24 h (77%); (b) 4-aminophenol or 5-aminopyridin-2-ol, Cs₂CO₃, DMSO, microwave, 150 °C (77%); (c) PdCl₂(*t*-Bu₂PhP)₂, CH₃COOK, ACN/H₂O, 85 °C, 15 h (91%); (d) 5-aminopyridin-2-ol hydrochloride, Cs₂CO₃, DMF, 100 °C, 24 h (56%); (e) 3-chloro-6-phenylpyridazine, PPTS, *s*-BuOH, 100 °C, 1 h (43%); (f) *s*-BuOH, *t*-BuOH, or DMSO, ~100 °C 1–16 h (14–93%); (g) R-B(OH)₂, PdCl₂(dppf), Na₂CO₃, H₂O, dioxane, 100 °C, 1.5 h (10–30%).

mechanisms other than AK inhibition; for example, **1** and **2** have demonstrated clinical efficacy against T315I Bcr-Abl-mutated CML.¹⁰ Off-target activities may also lead to dose-limiting adverse events unrelated to AK inhibition, for example, hypertension observed with the antiangiogenic AurA inhibitor **7** (ENMD-2076).¹¹ Our aim was to test unconfounded clinical effects of AK inhibition; hence a clinical candidate would require at least comparable kinase selectivity to **14b** for reasonable confidence that efficacy as well as dose-limiting toxicity would be on-mechanism.

Another feature of the phthalazine compounds that was deemed essential to preserve was their potency against MDR cell lines that overexpress P-glycoprotein (P-gp). In contrast to compounds **1**, **2**, and **3b** (AZD1152-HQPA⁹),¹² many of the phthalazines possessed comparable potency against the doxorubicin-selected P-gp-overexpressing uterine sarcoma cell line MES-SA DxS¹³ relative to their potency against non P-gp-expressing cell lines such as the parental MES-SA or HeLa cells. For example, compound **14a** suppressed phosphorylation of the AurB substrate Histone H3 (p-HH3) with a 24 h IC₅₀ of 11 nM in MES-SA DxS cells, which is comparable to its average EC₅₀ (15 nM) for induction of polyploidy in HeLa cells.⁶ In transport studies using MDR1-LLC-PK1 cells, the AKIs **2** and **3** showed poor passive permeability, and **1** had a high efflux ratio (>43).¹⁴ It is plausible that the strongly basic amines of these AKIs promote transport-mediated efflux and a resulting loss of potency in MDR cells.¹⁵

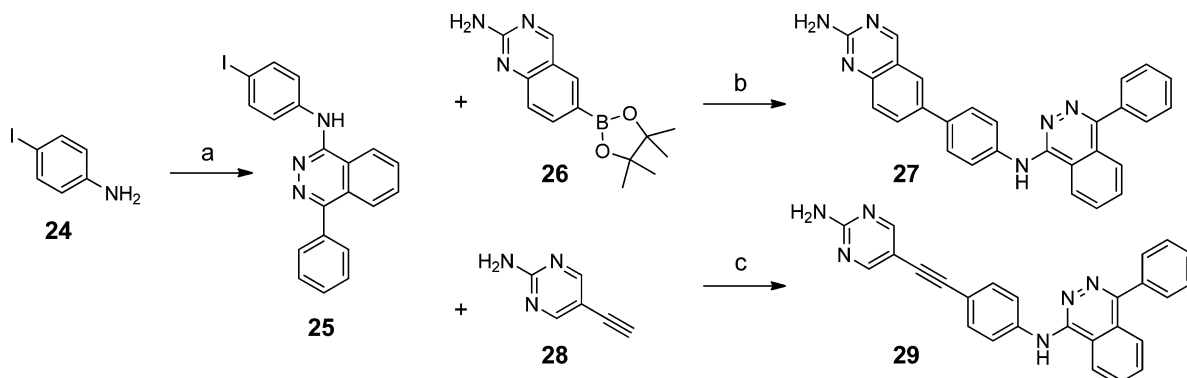
Cytotoxic agents are commonly dosed intravenously. However, we hypothesized that the ability to dose on multiple consecutive days may be important for clinical efficacy of a reversibly binding agent that can target cells only when they are

in the mitotic phase of the cell cycle. Toward that end, the good oral bioavailability of the phthalazine AKIs would be another characteristic to retain.

Despite the promising features of compounds such as **14a** and **14b**, we were concerned that their marginal solubility (<8 µg/mL in PBS, pH 7.4) and fast in vitro metabolism [>80% turnover upon 30 min incubation with human or rat liver microsomes (HLM or RLM)] could present a challenge for achieving sufficient exposure in the clinic. On the other hand, for a cytotoxic agent a moderate in vivo half-life (<4 h) may be an advantage, providing good control over the duration of exposure. Given uncertainty about the optimal level and duration of AurB inhibition, flexibility was key. Perhaps it would be desirable to have 24 h coverage of the target with a single dose in humans, but with a schedule involving dosing over many days, it could also turn out to be useful to enable pulsatile coverage (AurB inhibition for a fraction of each day).³¹ Therefore, we did not seek a long half-life in order to obtain extended inhibition of the Aurora kinases. Rather, reduction of the dose required to achieve significant daily target coverage was pursued through a variety of means (such as increasing potency and reducing metabolism) in order to minimize formulation/pharmacokinetic risk related to the marginal solubility of these compounds.

RESULTS AND DISCUSSION

Chemistry. Enaminone **15**³² was condensed with guanidine to provide 2-chloropyridine derivative **16**, which was then reacted with 4-aminophenol to produce aniline intermediate **20a**. The respective aminopyridine intermediate **20b** was best

Scheme 2. Synthesis of Truncated *N*,4-Diphenylphthalazin-1-amines^a

^aReagents and conditions: (a) 1-chloro-4-phenylphthalazine, 110 °C, overnight (88%); (b) PdCl₂(dppf), Na₂CO₃, H₂O, dioxane, 90 °C, overnight (52%); (c) CuI, (PPh₃)₂PdCl₂, ACN/TEA, 90 °C, overnight (52%).

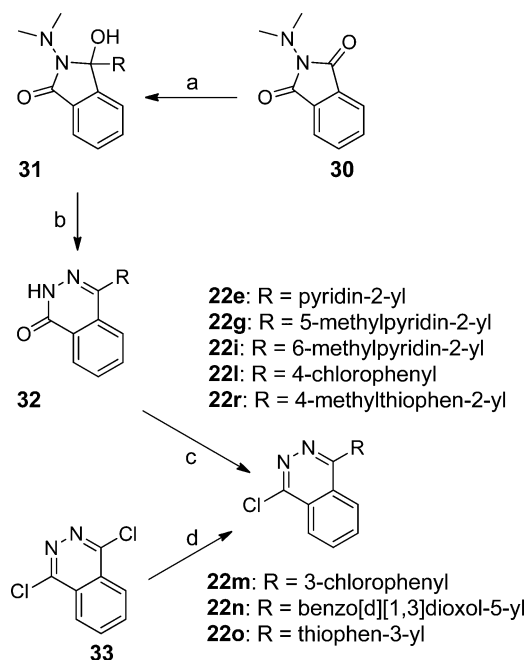
prepared from S_NAr reaction of 5-aminopyridin-2-ol with the more electrophilic 2-fluoropyridine reagent 19, which itself was obtained by Suzuki coupling of 4-chloropyrimidin-2-amine 17 and 2-fluoropyridine-3-boronic acid 18. 20a was then reacted with 3-chloro-6-phenylpyridazine to produce pyridazine compound 21; similarly, 20a or 20b underwent S_NAr with a variety of chlorophthalazines 22 to produce phthalazinamines 23. Alternatively, Suzuki reaction of chlorophthalazine 23b with an appropriate boronic acid provided 23k, 23p, and 23q (Scheme 1).

Iodophenyl phthalazinamine reagent 25 was generated by reacting 4-iodoaniline with 1-chloro-4-phenylphthalazine 22c. Suzuki reaction with boronic ester 26³³ or Sonogashira coupling with alkyne 28³⁴ provided quinazoline 27 and alkyne 29, respectively (Scheme 2).

The syntheses of chlorophthalazines 22g, 22i, 22l, and 22r have been described previously,³⁵ and 22e was obtained by the three-step procedure from *N,N*-dimethylaminophthalamide that is described in this work (Scheme 3). A process chemistry route to 22r has also been published.³⁶ 22m, 22n, and 22o were provided by Suzuki reaction of 1,4-dichlorophthalazine with an appropriate boronic ester (Scheme 3).

DISCUSSION

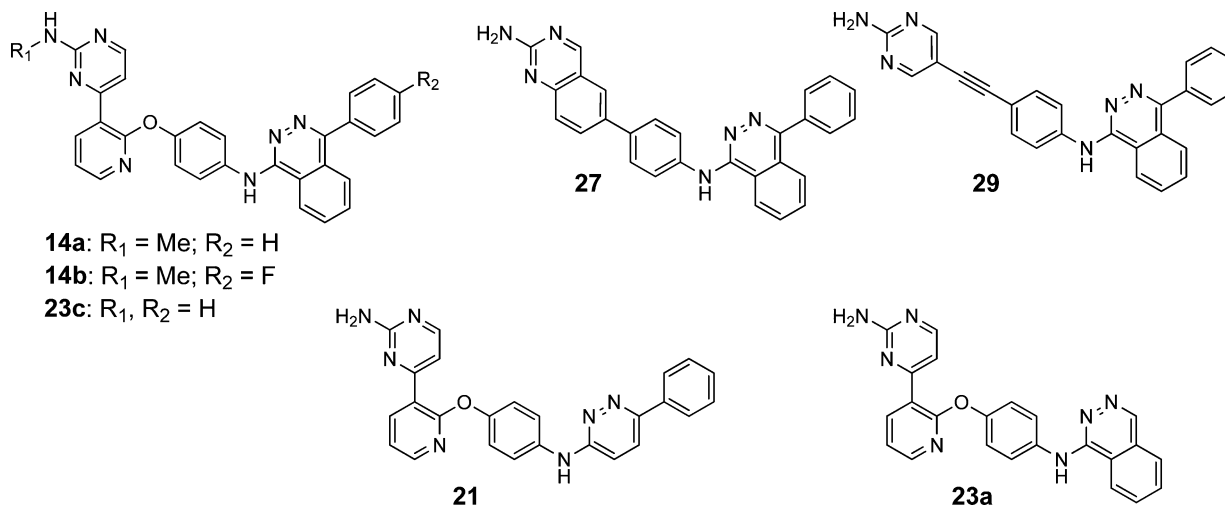
Compound 14a⁶ (Table 2) is relatively large (MW 498); therefore, SAR studies began by assessing the potency contributions of various portions of this scaffold in order to remove any atoms that were not critical for potency. The first modification was productive: removal of the methyl group on the aminopyrimidine provided a 5-fold improvement in cellular potency (14a → 23c). Next, we pursued other structural modifications to reduce MW.³⁴ Truncation of the kinase hinge-binding region of pyridyl pyrimidine 14a produced quinazoline 27 and alkynyl pyrimidine 29, both of which maintained single-digit AurB enzyme potency (Table 2). However, in contrast to compound 23c, the smaller variants 27 and 29 did not induce an AurB inhibitory phenotype (polyploidy) in a cellular assay at concentrations up to 1200 nM (Table 2). Other truncations aimed at reducing MW provided compounds 21 and 23a; while a 2–3-fold loss of AurB enzyme activity relative to 23c was observed, cellular AurB phenotype activity was attenuated by 43- and 160-fold, respectively, indicating that the fused and pendant aryl rings of the phthalazine were also necessary for high cellular potency.

Scheme 3. Synthesis of 4-Substituted 1-Chlorophthalazines^a

^aReagents and conditions: (a) R-Br, *n*-BuLi, THF, −78 °C → rt, or 3-methylthiophene, *n*-BuLi, TMEDA, Et₂O, reflux → rt (65–86%); (b) H₂N–NH₂, EtOH, reflux, overnight (81–98%); (c) POCl₃, reflux, 18 h (32–99%); (d) R-B(OH)₂, PdCl₂(dppf), Na₂CO₃, H₂O, dioxane, 90–100 °C, 1–16 h (21–68%).

Compounds 23c, 27, and 29 demonstrated good passive permeability and low efflux in MDR1-LLC-PK1 cells, which suggested that the absence of cellular potency for the latter two compounds was not related to poor cell penetration. In fact, AurB “false positives”, compounds that showed strong inhibition of AurB in the enzyme assay and little or no potency in an AurB cellular assay (despite independent evidence of good cell penetration), were frequently encountered in the original AurB HTS screen, in early lead optimization efforts, and also in counterscreening efforts for other kinase inhibitor programs. A plausible explanation for this phenomenon is that AK enzyme assays may fail to capture the intrinsic potency of compounds in their cellular context, where they exist in multiprotein complexes that include the activating partners TPX2 (AurA)³⁷ and INCENP (AurB).³⁸ Although 27 and 29

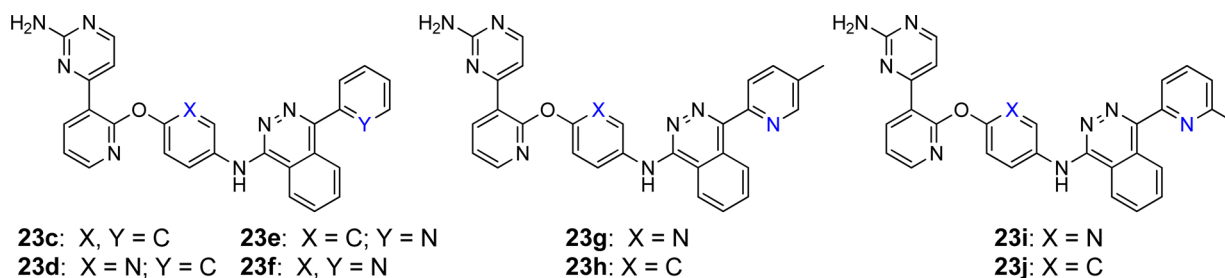
Table 2. Efforts to Reduce Molecular Weight



compd	MW	AurA/TPX2 ^a (IC ₅₀ , nM)	AurB ^a (IC ₅₀ , nM)	HeLa DNA ploidy ^b (EC ₅₀ , nM)	$P_{\text{appA} \rightarrow \text{B}}^c$ ($\times 10^{-6}$ cm/s)	efflux ^c ratio	AurA; AurB (Ambit K _d , nM) ¹⁶
14a	498	150 \pm 310	22 \pm 29	15 \pm 10	nd ^d	nd	nd
14b	516	41 \pm 13	15 \pm 14	24 \pm 25	nd	nd	nd
23c	484	32 \pm 24	5 \pm 5	3 \pm 3	11	1.5	6; 4
27	441	160 \pm 3	4 \pm 5	>1200	8.5	1.6	250; 12
29	414	590 \pm 220	8 \pm 2	>1200	10	0.9	710; 33
21	433	280 \pm 3	15 \pm 1	130	nd	nd	nd
23a	407	1100 \pm 11	12 \pm 2	490	nd	nd	nd

^aAll kinase assays were run at the K_m for ATP and represent an average of at least two determinations. ^bHeLa cellular assay with 10% FBS, Cellomics, $\geq 4\text{N}$ DNA content at 24 h. EC₅₀ values <25 nM represent an average of at least three determinations; the others are single determinations. ^cApparent permeability, apical to basolateral velocity and efflux ratio in hMDR1-LLC-PK1 cells. ^dnd: not determined.

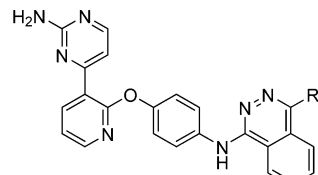
Table 3. Effects of Nitrogen Substitution on Protein Binding, Cellular Potency, and Pharmacokinetic Parameters

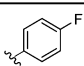
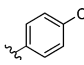
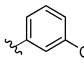
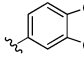
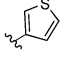
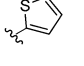
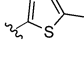
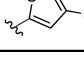


ID	properties		cellular potency (nM)		hMDR1-LLC-PK1	protein binding/metabolism		rat PK		
	PSA (Å ²)	Log P ^a	HeLa DNA ploidy ^b (EC ₅₀)	MES-SA parental \rightarrow Dx5 p-HH3 ^c (IC ₅₀)	$P_{\text{appA} \rightarrow \text{B}}^d$ ($\times 10^{-6}$ cm/s); [ER]	human PPB ^e (%)	turnover (RLM; HLM ^f , %)	CL ^g (L/h/kg)	MRT ^g (h)	F ^h (%)
23c	112	3.9	3 \pm 3	2.4 \rightarrow 3.5	11; [1.5]	>99.9	93; 94	1.0	0.5	65
23d	125	3.4	4 \pm 3	1.8 \rightarrow 3.9	7.7; [6.6]	99.4	92; 18	2.2	0.7	25
23e	125	3.0	27 \pm 1	34 \rightarrow 64	15; [2.8]	99.2	46; 32			
23f	138	2.3	59 \pm 25	75 \rightarrow 400	3.0; [16]	96.0	38; 13			
23g	138	3.0	2	5.0 \rightarrow 25	3.2; [19]	96.8	63; 32	4.6	0.3	
23h	125	3.4	4	4.3 \rightarrow 11	18; [3.3]	99.4	51; 36	0.68	0.6	0
23i	138	2.9	5 \pm 4	10 \rightarrow 26	3.5; [19]	97.0	50; 15	1.1	0.4	
23j	125	3.4	6 \pm 2	6.0 \rightarrow 15	12; [2.2]	99.4	64; 20	0.35	0.7	33

^aMeasured Log P based on LC/UV/MS.⁴³ ^bHeLa cellular assay with 10% FBS, Cellomics, $\geq 4\text{N}$ DNA content at 24 h. Each IC₅₀ represents the average of at least two determinations except for **23g** and **23h** ($n = 1$). Values returned as < x are excluded from averages and are listed in the Supporting Information. ^cMES-SA [parental and Dx5 (doxorubicin-selected)] cellular assay with 10% FBS, Cellomics, p-HH3 at 24 h. Each IC₅₀ represents the average of two independent experiments run in duplicate ($n = 4$). For standard deviations, see the Supporting Information. ^dApparent permeability, apical to basolateral velocity; efflux ratio in brackets. ^eHuman protein binding, equilibrium dialysis. ^fRat and human LM, % = percent substrate disappearance at 30 min. In vivo experiments were carried out with male Sprague–Dawley rats ($n = 3$). ^giv, 0.25 mg/kg for **23c**, 0.5 mg/kg for all others. Vehicles: 10% EtOH, 20% PEG400, 20% propylene glycol, 50% water for **23d**; 100% DMSO for all others. ^hpo, 2 mg/kg. Vehicle: 1% Tween 80/2% HMPC, pH 2.2.

Table 4. Phthalazine Substituent SAR with Regard to Cellular Potency and PK Parameters in Rats



ID	R	Cellular potency (nM)		Microsomal metabolism	Rat PK			
		HeLa DNA ploidy ^a (EC ₅₀)	MES-SA parental→Dx5 p-HH3 ^b (IC ₅₀)	Turnover (RLM; HLM, % ^c)	CL ^d (L/h/kg)	MRT ^d (h)	F ^e (%)	Solubility 0.01 N HCl (mg/mL) ⁴⁴
23k		3±2	2.5→4.6	90; 34	0.70	1.3	57	>0.2
23l		< 2	2.6→4.5	81; 43	0.70	0.7	16	0.10
23m		5	--	93; 45	1.3	0.4	27	0.15
23n		< 2	1.4→2.1	82; 56	0.15	1.6	79	0.08
23o		15±12	--	95; 63	1.1	0.8	75	>0.2
23p		7	--	93; 49	0.2	0.6	24	0.16
23q		2±1	--	92; 82	1.1	0.9	--	--
23r		3±2	1.9→2.3	82; 51	1.0	0.5	73	>0.2

^aHeLa cellular assay with 10% FBS, Cellomics, ≥4N DNA content/cell at 24 h. Each IC₅₀ represents the average of at least two determinations except for **23n** and **23p** ($n = 1$). Values returned as < x are excluded from averages and are listed in the Supporting Information. ^bMES-SA [parental and Dx5 (doxorubicin-selected)] cellular assay with 10% FBS, Cellomics, p-HH3 at 24 h. Each IC₅₀ represents the average of two independent experiments run in duplicate ($n = 4$). For standard deviations, see the Supporting Information. ^cRat and human LM, % = percent substrate disappearance at 30 min. In vivo experiments were carried out with male Sprague–Dawley rats ($n = 3$). ^div, 0.5 mg/kg. Vehicles: 10% EtOH, 20% PEG400, 20% propylene glycol, 50% water for **23r**, DMSO for all others, ^epo, 2 mg/kg (**23l**, **23m**, **23n**) or 5 mg/kg (**23k**, **23o**, **23p**, **23r**). Vehicles: 1% Tween 80/2%HMPC pH 2.2 (**23l**, **23m**, **23n**, **23r**) or OraPlus pH 2 (**23k**, **23o**, **23p**).

showed AurB enzymatic potency similar to **23c**, both showed marginal potency relative to **23c** in an AurA enzyme assay in which the kinase is complexed with a peptide portion of its activating partner protein (TPX2) (Table 2). However, for this set of compounds, the apparent selectivity in favor of AurB vs AurA remained when TPX2 was removed as a variable (competitive binding K_d values¹⁶), thus leaving the “real” selectivity unclear, as well as the extent to which the AurA assay was improved by use of partner protein peptide. Other AKI drug discovery programs have relied on Aurora kinases complexed to partner peptides in order to more closely approximate the cellular context.^{9,21} The medicinal chemistry effort that culminated in **13a** (MLN8054)²⁹ was guided primarily by high throughput cellular assays.³⁹ Because of the high “false positive” rate using enzyme data, we found that it was crucial to focus on cellular data in order to interpret SAR. For simplicity, AK enzyme data is omitted from the tables that follow but is available in the Supporting Information.

In addition to the strategy of decreasing MW, we sought to decrease lipophilicity toward the aim of reducing metabolism⁴⁰ and improving physical properties and therefore investigated

whether phenyl rings could be replaced by pyridines (Table 3). In HeLa cells, a nitrogen in the central ring (**23d**) at position X provided comparable potency to carbon (**23c**), whereas a nitrogen in the terminal ring (at Y) sacrificed potency by 9-fold (**23c** → **23e**) or 15-fold (**23d** → **23f**). However, potency could be restored by introduction of a *meta*- or *para*-methyl group on the terminal pyridine ring (compounds **23g**–**23j**).

Despite potency in HeLa cells, nitrogen substitution had moderate costs with regard to potency in an MDR cell line (MES-SA Dx5)¹³ relative to parental cells (MES-SA) that do not overexpress P-gp. Dose–response curves for inhibition of p-HH3 in the two cell lines were determined in parallel on a set of compounds that included **23g**–**c**. The experiment was performed twice in duplicate, resulting in IC₅₀s that for all compounds in Table 3 were significantly higher in the MDR cells relative to parental cells ($p < 0.02$, Student's t test, two-tailed). Introduction of one N increased PSA from 112 to 125 Å² and provided IC₅₀ values 1.9–2.5-fold higher in MES-SA Dx5 cells relative to MES-SA cells (**23d**, **23e**, **23h**, **23j**). For compounds having two substitutions of N for C the PSA increased to 138 Å² (**23f**, **23g**, and **23i**) and the potency shifts

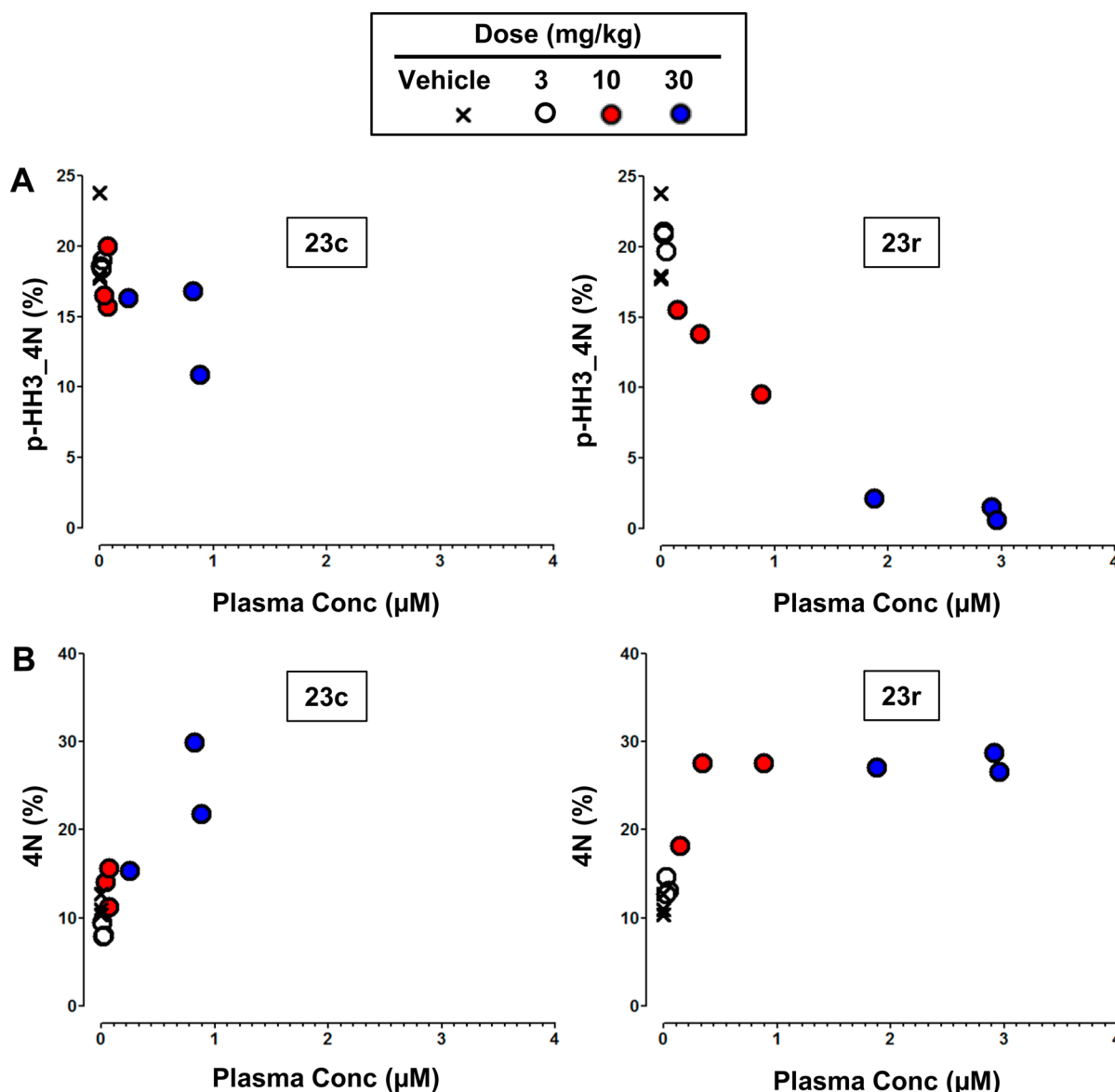


Figure 1. Pharmacodynamic response of compounds **23c** and **23r** 6 h after a single oral dose in female mice (individual animal data shown, 3, 10, and 30 mg/kg; $n = 3$ each group). Bone marrow cells were collected and processed for analysis by flow cytometry. (A) Suppression of p-HH3 in bone marrow cells gated for 4N DNA content versus plasma concentration. (B) Percentage of cells containing 4N DNA versus plasma concentration.

from parental line to MES-SA Dx5 were 2.6–5.3-fold. These compounds were likely P-gp substrates, with efflux ratios ≥ 16 in h-MDR1-transfected LLC-PK1 cells. It is plausible that their high average permeabilities ($\geq 25 \times 10^{-6}$ cm/s) contributed to keeping potency shifts in a moderate range. However, the quantitative relationship between transporter-mediated efflux in cancer cell lines and loss of clinical efficacy remains unclear.⁴¹ Our aim was to remove P-gp-mediated efflux as a potential clinical variable by advancing a compound for which a potency shift into MES-SA Dx5 cells was less than 2-fold.

Still, several compounds were further characterized in vitro and in vivo to gain an understanding of the SAR of metabolism and plasma protein binding (PPB) and to assess whether any of them were acceptable for evaluation in an in vivo pharmacodynamic (PD) assay. There was a clear impact of increased polarity on protein binding: in contrast to **23c**, compounds with PSA of 125 Å² had measurable fraction unbound (F_u) in human plasma (0.6–0.8%), and compounds with PSA of 138

Å² had human plasma F_u values of 3–4%. With regard to PK properties, nitrogen at position Y reduced intrinsic CL in RLM (compounds **23e–j** relative to **23c,d**). However, in vitro metabolic clearance did not correlate well with in vivo rat CL for the chemical series.

Compound **23j** had measurable plasma F_u (assuming comparable human and rat values) and reduced in vivo CL. Therefore, its unbound clearance (CL/F_u) was significantly lower than that of **23c**, albeit by a factor that cannot be quantified given the unmeasurably low plasma F_u of **23c**. On the other hand, because the cell assays (HeLa/MES-SA) were run in complete media containing 10% fetal bovine serum (FBS), it is likely that **23j** was considerably more free under the assay conditions than **23c**; thus the ratio of the “true” IC_{50} s ($23j\ IC_{50_unbound}/23c\ IC_{50_unbound}$) is probably higher than the ratio of the respective measured IC_{50} s.⁴² Assessment in a PD assay would be required to determine whether the reduced free in vivo CL of **23j** would translate into an advantage that could

override its potency disadvantage, including its moderate potency shift (2.5-fold) in MES-SA Dx5 vs parental cells.

In parallel work, various nonpyridine substituents on the phthalazine were explored in an effort to increase cellular potency (Table 4). Following on the observation that lipophilic substituents provided potency gains for pyridine compounds **23g–j**, the terminal phenyl of compound **23c** was substituted with halogen atoms. No significant increase in potency was observed, and the Cl-substituted compounds **23l** and **23m** demonstrated somewhat reduced solubility at pH 2 relative to compound **23c** (0.10 and 0.15 mg/mL versus >0.20 mg/mL) and reduced oral exposure in rats ($F\%$ = 16 and 27), respectively. Interestingly, despite poor solubility, benzodioxolane compound **23n** showed good oral absorption. While the low in vivo CL and high bioavailability of **23n** were attractive, the compound was a potent CYP3A4 inhibitor (IC_{50} = 210 nM) and therefore not a good clinical candidate. Thiophenes also were explored as replacements for the terminal phenyl ring (**23o–r**). Methyl-substituted thiophenes **23q** and **23r** provided greater potency than unsubstituted analogues **23o** and **23p**. Despite its high HLM CL, 4-methyl-2-thienyl compound **23r** showed acceptable in vivo pharmacokinetics in rats and was selected for in vivo assessment based on its potency against MES-SA Dx5 cells.

Phosphorylation of histone H3 in bone marrow cells was measured in the PD model as a surrogate tissue indicator of in vivo activity against AurB. Mice were administered compounds **23c** and **23r** orally at 3, 10, and 30 mg/kg. Six hours after a single dose of **23r** or vehicle control, the percentage of bone marrow cells with 4N DNA content and the level of p-HH3 in this cell subset were quantified by flow cytometry. Compound **23c** showed no significant suppression of p-HH3 (Figure 1A). In contrast, compound **23r** demonstrated significant ($p < 0.02$) inhibition of p-HH3 at a 10 mg/kg dose and complete suppression ($p < 0.001$) with a 30 mg/kg dose (Figure 1A), with a good dose/exposure relationship and plasma concentrations that were higher than for **23c** at the same doses. Both compounds exhibited a dose-dependent increase in the percentage of bone marrow cells with 4N DNA content (Figure 1B), which for compound **23c** is evidence that inhibition of AurB was likely achieved at time points earlier than 6 h postdose.⁴⁵

As expected based on its lack of nitrogens in the central and terminal rings, compound **23r** exhibited high PPB (>99.9% in mouse, rat, dog, monkey, and human). Compound **23j**, with its half-percent free fraction and lower rat IV CL, was judged to have the potential to provide greater potency in vivo. The two compounds were compared in a 6 h bone marrow PD study (**23j** with a highest dose of 15 mg/kg, **23r** at 15 mg/kg). In this experiment, **23r** provided 96% suppression of p-HH3 in 4N cells 6 h after dosing, with an average plasma total concentration of 3.0 μ M at that time point, but **23j** at 15 mg/kg provided a 6 h total plasma concentration of only 0.65 μ M and at that level failed to show significant evidence of AurB inhibition biochemically (p-HH3) or phenotypically (percentage of 4N cells).⁴⁶

Profiling of 23r. Robust and consistent performance of **23r** in the PD assay prompted us to characterize it in greater depth. As described above, two features of **14a** and **14b** that were deemed essential to preserve in a clinical candidate were high selectivity against other kinases and potency against MDR cell lines. Data for **23r** demonstrating these attributes has been published: in a panel of 26 kinases, only p38 α and TYK2

enzymes returned IC_{50} values <500 nM (TYK2, 220 nM; p38 α ,⁴⁷ 53 nM).¹² Upon further screening at 1 μ M in Ambit's competitive binding assays, 340 out of 353 nonmutant kinases returned % of control values >20 [a cutoff value corresponding to estimated $K_d \sim 250$ nM [$\text{Conc} \times (\text{POC}) / (1 - \text{POC})$]].⁴⁸ Of the remaining kinases, non-Aur kinases that returned follow-up K_d values <100 nM were: DDR1 (2 nM), LTK (13 nM), DDR2 (31 nM), FES (61), and Tie-1 (97 nM).¹²

With regard to cellular activity, remarkably consistent potency was observed across 26 tumor cell lines in a cell count imaging assay, including several MDR cells.¹² Table 5

Table 5. Potency of 23r and Three Clinical AurB Inhibitors against Sensitive and MDR Cell Lines^a

compd	cell count, EC_{50} at 72 h (nM)				
	CAL51 (breast)	MES-SA Dx5 (uterine)	HCT15 (colon)	SNU449 (liver)	769P (renal)
23r	2	1	2	2	2
1	21	>625	>625	>625	242
2	58	>625	>1250	>1250	>625
3b	54	>313	>313	>313	>313

^aFluorescence-based cell count imaging assay (ArrayScan VTI); cells in complete media (with 10% FBS) were treated for 24 h, washed twice, and incubated in complete media lacking inhibitor for 48 h. The assay was run in duplicate.

compares a smaller set of potency data for **23r** to EC_{50} values for benchmark clinical AKIs **1**, **2**, and **3b**. In contrast to **23r**, the benchmarks show significantly less potency in the MDR cells than in the sensitive cell line CAL51. Similar results were obtained for **23r** and the three benchmark compounds in 24 h assays measuring p-HH3 inhibition or DNA ploidy in cell lines that overexpress P-gp or BCRP.¹²

23r thus demonstrated a desirable in vitro potency and selectivity profile in addition to promising in vivo potency. However, given that its free fraction in plasma was unquantifiably low, it was crucial to investigate the extent to which any species differences in free fraction might impact projections of human in vivo potency and pharmacokinetics. To that end, suppression of p-HH3 in Jurkat cells was measured 3 h after incubation with compound **23r** and serum (5% and 25%, Table 6).⁴⁹ **23r** potency values with 5% and 25% serum were in good agreement across the species, which provided confidence that PPB differences would not be a significant confounding variable in predicting human pharmacokinetics and also that a given total plasma concentration of

Table 6. Cross-Species Effect of Serum Addition on in Vitro Cellular Potency of Compound 23r^a

species	3 h p-HH3 suppression (Jurkat, IC_{50} (nM))		
	5% serum	25% serum	potency shift
mouse	42	189	4.5×
rat	48	176	3.7×
dog	59	273	4.6×
monkey	24 \pm <1	111 \pm 4	4.6×
human	54 \pm 13	208 \pm 61	3.9×

^a**23r** was preincubated with serum for 60 min and then Jurkat cells were exposed to **23r**/serum for 3 h. p-HH3 IC_{50} values were determined using a Cellomics ArrayScan VTI. Monkey and human serum were evaluated in two independent experiments.

23r would provide comparable AurB inhibition in mice and humans.

It is notable that the IC_{50} values in the serum shift assay (Table 6) are high relative to the 2–3 nM potency of **23r** in phenotypic and biochemical cellular assays (Table 4). This perhaps suggests slow binding kinetics, given that the serum shift was a 3 h assay rather than 24 h as in the other cellular assays. Indeed, a time-dependence for apparent cellular potency of **23r** is captured in a time course experiment measuring the suppression of p-HH3 in Jurkat cells (Figure 2); the 24 h IC_{50}

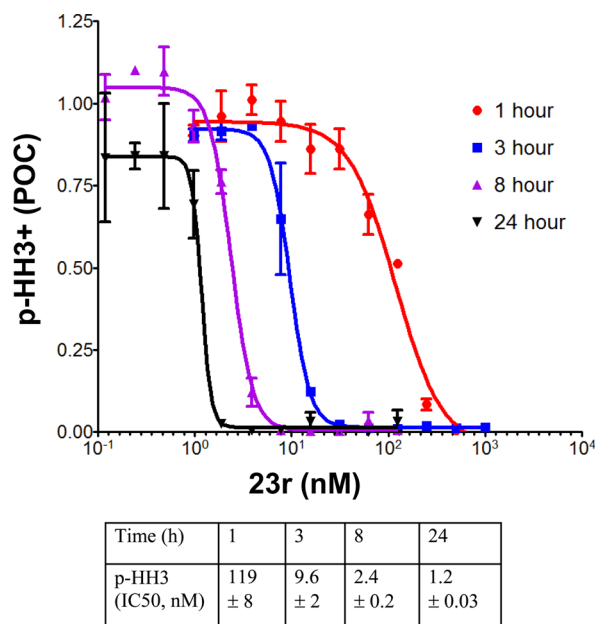


Figure 2. Time-dependent cellular potency of **23r**. Jurkat cells in complete media with 10% FBS were treated with **23r** for the indicated time intervals, and suppression of p-HH3 was measured by fluorescence-based imaging assay (ArrayScan VTi, duplicate experiments, error bars \pm SD).

for AurB inhibition by **23r** was only 2-fold lower than the 8 h IC_{50} , but it was 100-fold lower than the 1 h IC_{50} . The observed slow equilibration to maximal p-HH3 suppression could be the result of low permeability, slow binding to AurB (low k_{on}), or slow off-rates (low k_{off}) for binding to the experimental apparatus or proteins in the media. The good passive permeability of **23r** ($\sim 10 \times 10^{-6}$ cm/s in WT LLC-PK1 cells)¹⁴ is evidence against the first possible reason. Data below suggests that slow binding to AurB in cells is also unlikely (Figure 3).

Regardless of cause, the time-dependence of AK inhibition made it necessary to assess relative cellular potencies of **23r** against AurA versus AurB using the same duration of exposure. In experiments that were designed to maximize the percentage of cells in mitosis for optimal AurA activity signal, semi-synchronized cells released from G₁-S block 2 or 3 h prior were treated for 6 h with a concentration range of **23r** and IC_{50} values for suppression of p-HH3 and p-Aurora-A Thr²⁸⁸ (p-AurA) were determined (Table 7). In both HeLa and HCT-116 cells, **23r** inhibited biochemical activity of AurA and AurB with equal potency, providing 6 h IC_{50} values (4–8 nM) that were between the 3 and 8 h IC_{50} s of the Jurkat time-course experiment in Figure 2.

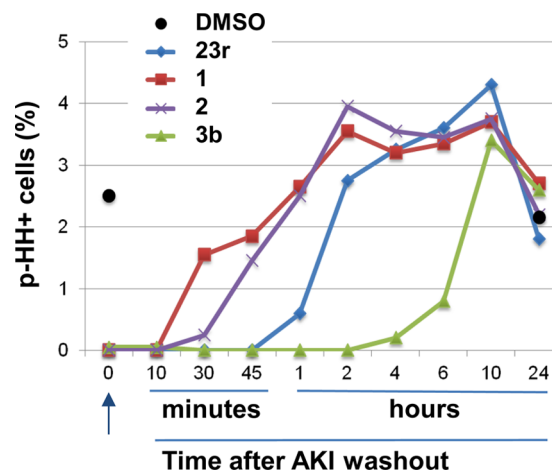


Figure 3. Jurkat cells in complete media with 10% FBS were treated for 3 h with compound at concentrations previously determined by Western blot to provide maximal inhibition of p-HH3+ signal: **23r** (250 nM), **1** (500 nM), **2** (1000 nM), **3b** (250 nM). After drug washout, cells were harvested at the indicated time intervals and assessed by flow cytometry for the percentage of p-HH3+ cells. Time zero is baseline level of p-HH3 suppression at 3 h post-treatment (arrow). DMSO p-HH3 level is indicated at 0 and 24 h time points. Data represents the mean p-HH3+ cells from two independent experiments.

Table 7. Equivalent Cellular Inhibition of AurA and AurB by **23r**^a

cell line	substrate detected	time (h)	IC_{50} (nM)
HeLa	p-AurA	6	7 ± 1
HeLa	p-HH3	6	8 ± 1
HCT-116	p-AurA	6	4 ± <1
HCT-116	p-HH3	6	4 ± <1

^aCells semisynchronized with thymidine were released from G₁-S phase and treated with **23r** in complete media with 10% FBS. Immunofluorescence imaging assay (ArrayScan VTi; Cellomics) was used to determine the mean fluorescence intensity of individual mitotic objects, independent experiments ($n = 2$).

Slow binding kinetics of **23r** to AurB was observed in an enzyme binding assay: the dissociation half-life was observed to be ≥ 2.6 h by surface plasmon resonance (Table 8). The resulting K_d was in agreement with the AurB K_d determined in Ambit's competition binding assay (1.5 nM) as well as the AurB enzyme IC_{50} (4 nM).

Table 8. AurB Enzyme Binding Kinetics for **23r**

k_{on} ^a ($M^{-1} s^{-1}$)	k_{off} ^b (s^{-1})	K_d (nM)	$t_{1/2}$ (h)	R_{max} (RU)
3.6×10^4	$\leq 7.3 \times 10^{-5}$	≤ 2.0	≥ 2.6	10.0

^aEnzyme kinetics were determined by surface plasmon resonance using a Biacore instrument. ^bA single determination provided the listed, statistically valid k_{off} value; multiple other experiments provided higher values that were flagged as unreliable by the Biacore T200 Evaluation software.

On the other hand, in a wash-out experiment with Jurkat cells, **23r** did not appear to have a slow AurB enzyme off-rate: the percentage of cells that were p-HH3 positive returned to baseline levels (Figure 3) 2 h after removal of **23r**, which is moderately longer than the time to restore p-HH3 levels after washout of AKIs **1** and **2**. In contrast, AurB-selective inhibitor

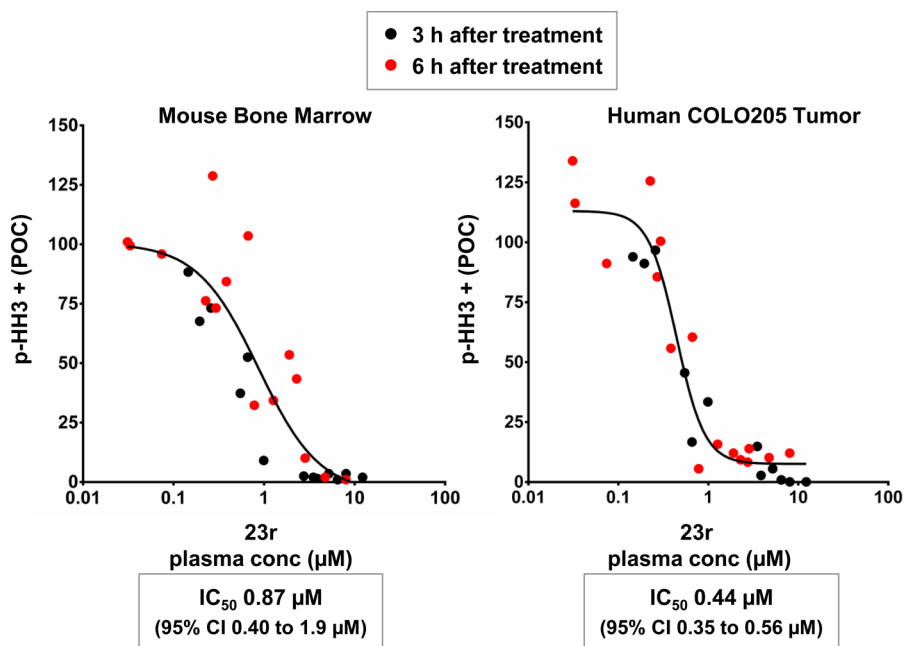


Figure 4. Athymic nude mice bearing human COLO205 tumors were treated with a single dose of 23r at 1.5, 3.5, 7.5, 15, and 30 mg/kg or vehicle control alone ($n = 3$ animals per dose group). Tumor and bone marrow samples were collected at 3 h (solid black circles) and 6 h (solid red circles) after treatment. IC₅₀ values were determined by plotting observed p-HH3+ cells in G2/M as a POC (y-axis) vs 23r concentration in plasma (x-axis) from individual animals. The vehicle control treatment group was used as the control [p-HH3+; bone marrow (mean 19.8, SD \pm 2.3), COLO205 tumor (mean 10.8, SD \pm 2.6)]. The predicted bone marrow and tumor p-HH3 IC₅₀ values in mouse plasma were 0.87 and 0.44 μ M, respectively.

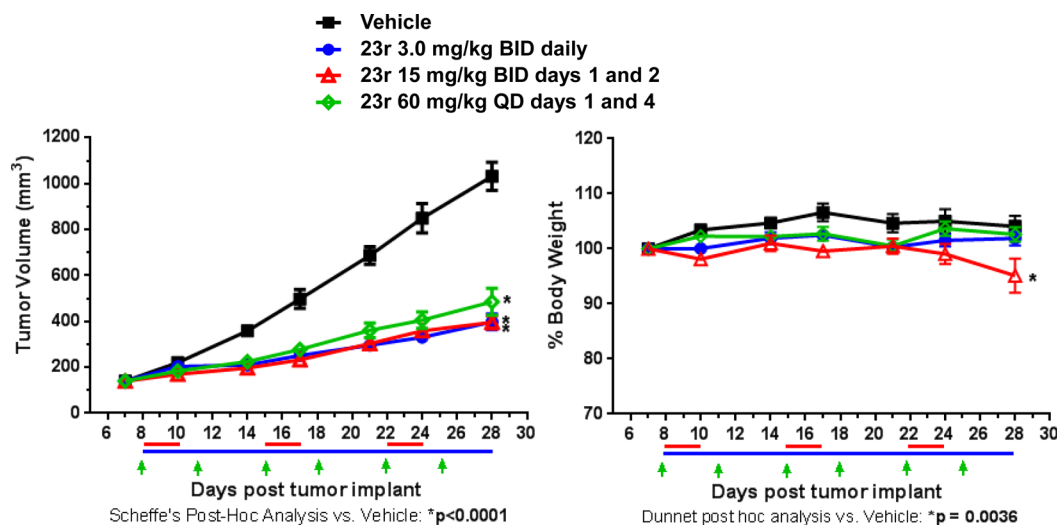


Figure 5. 23r inhibits the growth of HCT-116 tumor xenografts in vivo with daily or intermittent dosing schedules.

3b continued to suppress p-HH3 signal several hours after washout; inhibition of AurB activity by this AKI may be limited by the half-life of AurB itself, which is estimated to be only a few hours in cell culture.⁵⁰ AurB inhibitor 6 (GSK1070916)²¹ has been reported to have a very long residence time in AurB enzyme assays and to wash out of cells slowly.⁵¹ The authors note that extension of an AKI into the hydrophobic pocket adjacent to the ATP binding site is necessary but not sufficient for the slow-binding kinetics observed with 6 and related compounds. It is plausible that this hydrophobic pocket is also occupied by AKIs 5 (SNS-314),¹⁹ 9 (ABT-348),²⁵ 3a, and 23r. In any case, after 23r was washed out of the cells, the AurB-inhibitory activity decreased faster than may be expected based on the slow off-rate observed in the enzyme binding assay. This

apparent discrepancy may be another example of an AKI enzyme assay failing to capture the kinetics as well as thermodynamics of binding to the multiprotein complex that exists in cells. Also, as mentioned above, the lack of a slow AurB off-rate in cells suggests that a slow on-rate is unlikely to explain the time-dependent cellular potency of 23r.

The moderate residence time of 23r after wash out avoids one potential complication in the development of an understanding of PK/PD/efficacy/toxicity relationships. However, complexities around potential time dependence of binding to the AKs, plasma proteins, or assay surfaces show that it is not straightforward to estimate expected in vivo duration and intensity of target coverage by extrapolating from in vitro determinations of 23r potency. It would be important, then, to

further characterize the inhibition of AurB *in vivo*. To that end, mice bearing established COLO205 tumors were administered a single oral dose of vehicle alone or **23r** at 1.5, 3.5, 7.5, 15, and 30 mg/kg. Tumor and bone marrow samples that were taken 3 and 6 h after dosing were assessed for the percentage of p-HH3+ cells relative to that in control animals. As shown in Figure 4, the *in vivo* IC₅₀ for p-HH3 suppression in COLO205 tumors was determined to be about 0.44 μ M. The *in vivo* IC₅₀ in bone marrow cells was somewhat higher, but the confidence intervals between the two experiments overlapped. This and other PD experiments quantified the duration of time for which a given dose of **23r** in mice provides plasma concentrations that maintain at least 50% suppression of p-HH3. For example, from a PK/PD study examining p-HH3 inhibition in HCT-116 tumor xenografts by fluorescence-based microscopy, a single 3.75 mg/kg dose of **23r** was estimated to provide >50% inhibition of p-HH3 for 3–4 h, whereas a 7.5 mg/kg dose provided 6–8 h of target coverage, and 15 mg/kg inhibited p-HH3 for >9 h.¹²

These PD studies provided context for estimating the duration of AurB inhibition required for suppression of tumor growth *in vivo*. For example, in the study illustrated in Figure 5, mice bearing established HCT-116 tumors were orally administered vehicle alone or **23r** with three distinct doses and schedules (*n* = 10 animals for each group). On the basis of pharmacokinetic data for the lowest dose in the above study, daily dosing of **23r** at 3.0 mg/kg BID would provide >50% suppression of p-HH3 for roughly 6–8 h/day, target coverage that resulted in 71% tumor growth inhibition (TGI). Comparable TGI was observed with BID dosing of 15 mg/kg **23r** on two consecutive days of every week, a dosing scheme that is estimated to provide >18 h/day with plasma concentrations above the *in vivo* IC₅₀ of 0.44 μ M. A 60 mg/kg QD dose on days 1 and 4 of every week provided 61% TGI. Terminal PK of this group showed that 24 h after dosing a 60 mg/kg dose provided only 15 nM plasma concentration; therefore the duration of target coverage above the *in vivo* IC₅₀ provided by that dose was significantly less than 24 h. All dosing regimens with **23r** were well-tolerated with no adverse effects on body weight, except in the 15 mg/kg 2-consecutive-days group (average of 5%, which includes one mouse with >20% body weight loss). In all groups treated with **23r**, a decrease in neutrophil counts (25–50% of the vehicle-control group) was observed at the end of the study. In other studies, neutropenia induced by **23r** has been shown to be transient and reversible.¹²

The experiment above and tumor xenograft dose response studies reported earlier¹² demonstrate that preclinical efficacy is achieved from pulsatile inhibition of AurB activity by **23r**, and that this inhibition can occur with a variety of distinct schedules. Clearly **23r** is a suitable candidate compound for studying the pharmacodynamic/efficacy/toxicity relationship of AurB inhibition in mice. It is also well-suited for preclinical combination studies, for example, with PEGylated-granulocyte colony-stimulating factor to attenuate neutropenia¹² and microtubule-targeting agents⁵² or HDAC inhibitors⁵³ to enhance efficacy. Despite its high Log *P* (4.4),⁴³ limited solubility (1 μ g/mL in PBS at pH 7 and 360 μ g/mL in the acidic formulation listed in Table 4) and high *in vitro* metabolic intrinsic clearance, **23r** exhibited good pharmacokinetic properties in preclinical species and was predicted to have low CL (0.036 L/h/kg) and good oral absorption in humans.¹⁴ Therefore, we anticipated that a suitable salt form could

provide sufficient drug exposure to achieve efficacy in humans. On the basis of its potency, selectivity, dosing flexibility, and efficacy against MDR tumor cells and tumor xenografts,^{12,52} **23r** was selected as a development candidate for clinical trials.

CONCLUSION

We have described our path toward identifying an AurB phenotype inhibitor clinical candidate from advanced leads. These pyridinyl-pyrimidine phthalazines had features we intended to retain (oral bioavailability, high selectivity against other kinases, and relative potency against MDR cell lines) and some areas for improvement (potency, solubility, PPB, and metabolism). Efforts to reduce Log *P* and increase polarity by replacement of carbon with nitrogen did provide lower protein binding and better microsomal stability but at the expense of reduced potency in MDR cells. It was, however, possible to achieve improved potency, and **23r** was determined to be 5–8-fold more potent than advanced leads **14a/b**. Despite high *in vitro* metabolism, low solubility, and high PPB, **23r** proved to have best-in-series *in vivo* target coverage, efficacy in multiple tumor xenograft models at reasonable doses, and predicted human pharmacokinetics that suggested adequate target coverage could be achieved. **23r** is currently in phase 1 trials for evaluation in adult patients with advanced solid and hematological cancers. Human PK results have been consistent with predictions, and in dose expansion studies with G-CSF support, **23r** (AMG 900) has shown promising single-agent activity in heavily pretreated patients with taxane-resistant ovarian cancer as well as activity against other female reproductive cancers.⁵⁴ On the basis of strong preclinical and biomarker⁵⁵ data, combination studies in patients with these tumor types are planned.

EXPERIMENTAL SECTION

Unless otherwise noted, all materials were obtained from commercial suppliers and used without further purification. Anhydrous solvents were obtained from EMD or Aldrich and used directly. All reactions involving air- or moisture-sensitive reagents were performed under a nitrogen or argon atmosphere. Microwave-assisted reactions were conducted with a Smith synthesizer from Personal Chemistry (Uppsala, Sweden). Silica gel chromatography was performed using either glass columns packed with silica gel (200–400 mesh, Aldrich Chemical) or medium pressure liquid chromatography (MPLC) on a CombiFlash Companion (Teledyne Isco) with RediSep normal-phase silica gel (35–60 μ m) columns and UV detection at 254 nm. Preparative reversed-phase HPLC was performed on a Gilson (215 liquid handler), YMC-Pack Pro C18, 150 mm \times 30 mm I.D. column, eluting with a binary solvent system A and B using a gradient elution (A, H₂O with 0.1% TFA; B, CH₃CN with 0.1% TFA; gradient elution) with UV detection at 254 nm. All final compounds were purified to \geq 95% purity (94% for **23g**) as determined by Agilent 1100 series high performance liquid chromatography (HPLC) with UV detection at 254 nm using one of the following methods. Method A: Zorbax SB-C8, 4.6 mm \times 150 mm, 15 min; 1.5 mL/min flow rate; 0–100% 0.1% TFA in CH₃CN/0.1% TFA in H₂O. Method B: Phenomenex Synergi, 2 mm \times 50 mm, 3 min, 1.0 mL/min flow rate, 5–95% 0.1% formic acid in CH₃CN/0.1% formic acid in H₂O. Low-resolution mass spectral (MS) data were determined on an Agilent 1100 series LCMS with UV detection at 254 nm and a low resonance electrospray mode (ESI). NMR spectra were determined with either a Bruker AV-400 (400 MHz) spectrometer or a Varian 400 or 300 MHz spectrometer at ambient temperature. Chemical shifts are reported in ppm from the solvent resonance (DMSO-*d*₆ 2.49 ppm). Data are reported as follows: chemical shift, number of protons, multiplicity (*s* = singlet, *d* = doublet, *t* = triplet, *q* = quartet, *br* = broad, *m* = multiplet), and coupling constants. Differential scanning calorimetry (DSC) was

performed on a TA Instruments Q100 calorimeter at 10 °C/min from 30 to 300 °C in a crimped aluminum pan under dry nitrogen at 50 mL/min.

4-(2-Chloropyridin-3-yl)pyrimidin-2-amine (16). Sodium pellets (2.8 g, 123 mmol) were rinsed with hexanes and placed in a 500 mL round-bottomed flask fitted with an argon inlet and outlet. The flask was cooled to 0 °C, 100 mL of anhyd MeOH was added, and the reaction was stirred under argon. After most of the sodium had been consumed, the reaction was warmed to room temperature (rt) and an additional 30 mL of anhyd MeOH was added. After 15 min, guanidine hydrochloride (15 g, 152 mmol) was added and the mixture was stirred for 30 min. (*E*)-1-(2-Chloropyridin-3-yl)-3-(dimethylamino)-prop-2-en-1-one (10.0 g, 47 mmol) was added in one portion, and the yellow mixture was allowed to stir overnight. The reaction was fitted with an air-cooled reflux condenser and was heated to 50 °C for 16 h. The mixture was cooled and concentrated to a slurry, which was filtered, and the solid was rinsed with saturated NaHCO₃ and water. The solid was dried in vacuo to give the title compound (8.3 g, 85% yield) as a white solid. ¹H NMR (Bruker, 400 MHz, DMSO-*d*₆) δ: 8.51 (d, *J* = 4.4 Hz, 1H), 8.36 (d, *J* = 5.5 Hz, 1H), 8.01 (d, *J* = 7.3 Hz, 1H), 7.55 (m, 1H), 6.67 (s, 3H). MS Calcd for C₉H₇ClN₄: [M]⁺ = 206. Found: [M + H]⁺ = 207.

4-(2-Fluoropyridin-3-yl)pyrimidin-2-amine (19). A pressure bottle was charged with bis(*di-tert*-butyl(phenyl)phosphine)palladium dichloride (0.288 g, 0.463 mmol), potassium acetate (4.55 g, 46.3 mmol), 2-fluoropyridine-3-boronic acid hydrate (4.89 g, 34.7 mmol), and 4-chloropyrimidin-2-amine (3.00 g, 23.2 mmol) and was purged with nitrogen for several minutes. Water (12.5 mL, 695 mmol) and acetonitrile (93 mL) were added, the bottle was sealed, and the reaction mixture was heated at 85 °C for 15 h. The mixture was diluted with water and DCM, and the layers were separated. The organic portion was washed with saturated NaHCO₃, dried with Na₂SO₄, filtered, and concentrated. The resulting solid was triturated with ether and filtered to provide 4-(2-fluoropyridin-3-yl)pyrimidin-2-amine (4.02 g, 91% yield) as a light-yellow solid. ¹H NMR (400 MHz, DMSO-*d*₆) δ ppm 8.50 (1H, t, *J* = 8.0 Hz), 8.38–8.35 (2H, m), 7.55–7.52 (1H, m), 7.05–7.02 (1H, m), 6.83 (2H, br s). MS Calcd for C₉H₇FN₄: [M]⁺ = 190. Found: [M + H]⁺ = 191.

4-(2-(4-Aminophenoxy)pyridin-3-yl)pyrimidin-2-amine (20a). 4-(2-Chloropyridin-3-yl)pyrimidin-2-amine (15, 6.0 g, 29.0 mmol), 4-aminophenol (3.17 g, 29.0 mmol) and Cs₂CO₃ (18.9 g, 58.1 mmol) were suspended in 50 mL of DMSO under nitrogen in a resealable pressure vessel, and the mixture was heated to 130 °C overnight. After cooling to rt and diluting with water, the resulting precipitate was isolated by filtration, washed with water and diethyl ether, and dried under high vacuum to provide 4-(2-(4-aminophenoxy)pyridin-3-yl)pyrimidin-2-amine (7.5 g, 92%). ¹H NMR (Bruker, 400 MHz, CDCl₃) δ: 8.33–8.14 (m, 3H), 7.27 (d, *J* = 5.1 Hz, 1H), 7.20 (t, *J* = 4.8 Hz, 1H), 6.87–6.73 (m, 4H), 6.59 (d, *J* = 8.8 Hz, 2H), 4.98 (s, 2H). MS Calcd for C₁₅H₁₃N₅O: [M]⁺ = 279. Found: [M + H]⁺ = 280.

4-(2-(5-Aminopyridin-2-yloxy)pyridin-3-yl)pyrimidin-2-amine (20b). A pressure bottle was charged with 5-aminopyridin-2-ol hydrochloride (3.85 g, 26.3 mmol), 4-(2-fluoropyridin-3-yl)pyrimidin-2-amine (18, 5.00 g, 26.3 mmol), Cs₂CO₃ (21.4 g, 65.7 mmol), and 53 mL of DMF. The bottle was sealed, and the mixture was heated at 100 °C for 24 h. The mixture was diluted with 300 mL of water and extracted 4× with 500 mL of 95:5 EtOAc/iPrOH. The combined organics were dried with MgSO₄, filtered, and concentrated. The oil was then concentrated twice from 50 mL of toluene to remove remaining DMF. The resulting solid was triturated with 3:1 Et₂O/EtOAc. The solids were filtered, rinsed with Et₂O/EtOAc, and dried to provide 4-(2-(5-aminopyridin-2-yloxy)pyridin-3-yl)pyrimidin-2-amine (4.11 g, 56% yield) as a tan solid. ¹H NMR (400 MHz, DMSO-*d*₆) δ ppm 8.39–8.26 (2H, m), 8.18 (1H, t, *J* = 4.0 Hz), 7.60 (1H, d, *J* = 4.0 Hz), 7.31–7.20 (2H, m), 7.07 (1H, s), 6.91–6.84 (1H, m), 6.71 (2H, s), 5.19 (2H, s). MS Calcd for C₁₄H₁₂N₆O: [M]⁺ = 280. Found: [M + H]⁺ = 281.

N-(4-(3-(2-Aminopyrimidin-4-yl)pyridin-2-yloxy)phenyl)-6-phenylpyridazin-3-amine (21). A reaction tube was charged with

PPTS (225 mg, 895 μmol), 4-(2-(4-aminophenoxy)pyridin-3-yl)pyrimidin-2-amine (20a, 125 mg, 448 μmol), 3-chloro-6-phenylpyridazine (85 mg, 448 μmol), and 1.8 mL of butan-2-ol. The tube was sealed, and the mixture was heated at 100 °C for 1 h. The mixture was concentrated, dissolved in MeOH/DMSO, and purified by reverse phase chromatography (10–90% 0.1% TFA/ACN in 0.1% TFA/water over 14 min). The product-containing fractions were combined, washed with 1 M NaHCO₃, and extracted with EtOAc. The organic portion was dried with Na₂SO₄, filtered, and concentrated to provide N-(4-(3-(2-aminopyrimidin-4-yl)pyridin-2-yloxy)phenyl)-6-phenylpyridazin-3-amine (84 mg, 43% yield) as an off-white solid. ¹H NMR (400 MHz, DMSO-*d*₆) δ ppm 9.43 (1H, s), 8.36 (1H, d, *J* = 4.0 Hz), 8.34 (1H, d, *J* = 8.0 Hz), 8.21–8.20 (1H, m), 8.06–8.00 (3H, m), 7.83 (2H, d, *J* = 8.0 Hz), 7.53–7.44 (3H, m), 7.30–7.21 (3H, m), 7.16 (2H, d, *J* = 8.0), 6.74 (2H, br s). MS Calcd for C₂₅H₁₉N₇O: [M]⁺ = 433. Found: [M + H]⁺ = 434.

1-Chloro-4-(pyridin-2-yl)phthalazine (22e). Following the published procedure to prepare 1-chloro-4-(6-methylpyridin-2-yl)phthalazine,³⁵ 4-(pyridin-2-yl)phthalazin-1(2H)-one (31e, 110 mg, 493 μmol) and phosphorus oxychloride (230 μL, 2464 μmol) provided 1-chloro-4-(pyridin-2-yl)phthalazine (38 mg, 32% yield) as an off-white solid. ¹H NMR (400 MHz, DMSO-*d*₆) δ 8.86–8.84 (m, 1H), 8.67–8.65 (m, 1H), 8.42–8.40 (m, 1H), 8.23–8.10 (m, 4H), 7.68–7.64 (m, 1H). HRMS Calcd for C₁₃H₈ClN₂: [M + H]⁺ = 242.0480, [M + Na]⁺ = 264.0299. Found: [M + H]⁺ = 242.0496, [M + Na]⁺ = 264.0311.

1-Chloro-4-(3-chlorophenyl)phthalazine (22m). Following the general procedure described for 22o, 1,4-dichlorophthalazine and 3-chlorophenylboronic acid provided the title compound (266 mg, 21%) as an off-white solid. MS Calcd for C₁₄H₈Cl₂N₂: [M]⁺ = 274. Found: [M + H]⁺ = 275.

1-(Benzo[d][1,3]dioxol-5-yl)-4-chlorophthalazine (22n). Following the general procedure described for 22o, 1,4-dichlorophthalazine and benzo[d][1,3]dioxol-5-ylboronic acid provided the title compound (2.34 g, 68%) as a dark-red solid. ¹H NMR (Bruker, 400 MHz, DMSO-*d*₆) δ ppm 8.39–8.36 (1H, m), 8.21–8.17 (1H, m), 8.15–8.11 (1H, m), 8.11–8.08 (1H, m), 7.30 (1H, d, *J* = 1.6 Hz), 7.23–7.20 (1H, dd, *J* = 1.6, 7.9 Hz), 7.17–7.15 (1H, d, *J* = 7.9 Hz), 6.17 (2H, s). MS Calcd for C₁₅H₉ClN₂O₂: [M]⁺ = 284. Found: [M + H]⁺ = 285.

1-Chloro-4-(thiophen-3-yl)phthalazine (22o). 1,4-Dichlorophthalazine (3.1 g, 15.63 mmol), thiophen-3-ylboronic acid (1.0 g, 7.82 mmol), and Pd(dppf)Cl₂ (0.29 g, 0.39 mmol) were placed in a pressure-resistant vessel under argon and taken up in 1,4-dioxane (39.1 mL) and aq 2 M Na₂CO₃ solution (4.3 mL, 8.6 mmol). The resulting mixture was stirred at 90 °C for 16 h. After cooling to rt, the mixture was filtered over a Celite cake and rinsed with 1:1 EtOAc/DCM (100 mL). The filtrate was concentrated and purified by MPLC (20–40% EtOAc/Hexanes) to yield 1-chloro-4-(thiophen-3-yl)phthalazine (0.99 g, 4.0 mmol, 51% yield). ¹H NMR (Bruker, 400 MHz, DMSO-*d*₆) δ ppm 8.36–8.41 (m, 1H) 8.27–8.31 (m, 1H) 8.17 (m, 3H) 7.84 (m, 1H) 7.61 (dd, *J* = 4.9, 1.3 Hz, 1H). MS Calcd for C₁₂H₇ClN₂S: [M]⁺ = 246. Found: [M + H]⁺ = 247.

N-(4-(3-(2-Aminopyrimidin-4-yl)pyridin-2-yloxy)phenyl)-phthalazin-1-amine (23a). A reaction tube was charged with 4-(2-(4-aminophenoxy)pyridin-3-yl)pyrimidin-2-amine (20a, 125 mg, 448 μmol), 1-chlorophthalazine hydrochloride (90 mg, 448 μmol), and 2 mL of butan-2-ol. The tube was sealed, and the mixture was heated at 100 °C for 1 h. EtOAc was added to the cooled reaction mixture, and the resulting solids were filtered and rinsed with EtOAc. The crude solid was dissolved in DMSO/MeOH and purified by reverse phase chromatography (10–90% 0.1% TFA/ACN in 0.1% TFA/water over 14 min). The product-containing fractions were combined, and 1 M NaHCO₃ was added. The solids were filtered, washed with water, and dried to provide N-(4-(3-(2-aminopyrimidin-4-yl)pyridin-2-yloxy)-phenyl)phthalazin-1-amine (25 mg, 14% yield) as a light-yellow solid. ¹H NMR (400 MHz, DMSO-*d*₆) δ ppm 9.23 (1H, s), 9.13 (1H, s), 8.60 (1H, d, *J* = 8.0 Hz), 8.39–8.34 (2H, m), 8.23–8.22 (1H, m), 8.05–7.93 (5H, m), 7.31–7.27 (2H, m), 7.18 (2H, d, *J* = 4.0 Hz), 6.74

(2H, br s). MS Calcd for $C_{23}H_{17}N_7O$: $[M]^+ = 407$. Found: $[M + H]^+ = 408$.

N-(4-(3-(2-Aminopyrimidin-4-yl)pyridin-2-yloxy)phenyl)-4-chlorophthalazin-1-amine (23b). In a 75 mL pressure-resistant vessel, 4-(2-(4-aminophenoxy)pyridin-3-yl)pyrimidin-2-amine (**20a**, 0.90 g, 3.22 mmol) and 1,4-dichlorophthalazine (1.41 g, 7.09 mmol) were heated to 100 °C in butan-2-ol (16 mL) for 6 h. After cooling to rt, DCM (15 mL) was added and the resulting precipitate was filtered and dried in vacuo to yield **N**-(4-(3-(2-aminopyrimidin-4-yl)pyridin-2-yloxy)phenyl)-4-chlorophthalazin-1-amine (1.0 g, 2.26 mmol, 70% yield) as a tan solid. 1H NMR (Bruker, 400 MHz, DMSO- d_6) δ ppm 9.93 (br s, 1 H), 8.76–8.82 (m, 1 H), 8.35–8.48 (m, 3 H), 8.26–8.35 (m, 2 H), 8.19–8.24 (m, 1 H), 8.13–8.18 (m, 2 H), 7.85 (d, $J = 8.8$ Hz, 2 H), 7.51 (d, $J = 5.9$ Hz, 1 H), 7.35 (dd, $J = 7.6, 4.8$ Hz, 1 H), 7.27 (m, $J = 8.8$ Hz, 2 H). MS Calcd for $C_{23}H_{16}ClN_7O$: $[M]^+ = 441$. Found: $[M + H]^+ = 442$.

N-(4-(3-(2-Aminopyrimidin-4-yl)pyridin-2-yloxy)phenyl)-4-phenylphthalazin-1-amine (23c). Applying similar S_NAr conditions as for **23b**, 1-chloro-4-phenylphthalazine and **20a** in *t*-BuOH provided the title compound (120 mg, 70%) as an off-white solid: mp (DSC) 230 °C. 1H NMR (400 MHz, DMSO- d_6) δ ppm 9.33 (s, 1 H), 8.68 (d, $J = 7.82$ Hz, 1 H), 8.30–8.42 (m, 2 H), 8.23 (dd, $J = 4.74, 2.01$ Hz, 1 H), 7.86–8.09 (m, 5 H), 7.64–7.71 (m, 2 H), 7.48–7.63 (m, 3 H), 7.24–7.34 (m, 2 H), 7.19 (d, $J = 9.00$ Hz, 2 H), 6.74 (s, 2 H). HRMS m/z $[M + H]^+$ Calcd for $C_{29}H_{21}N_7O$: 484.1880. Found: 484.1882.

N-(6-(3-(2-Aminopyrimidin-4-yl)pyridin-2-yloxy)pyridin-3-yl)-4-phenylphthalazin-1-amine (23d). A pressure bottle was charged with 1-chloro-4-phenylphthalazine (2.1 g, 8.9 mmol), 4-(2-(5-aminopyridin-2-yloxy)pyridin-3-yl)pyrimidin-2-amine (**20b**, 2.5 g, 8.9 mmol), and 45 mL of DMSO. The bottle was sealed, and the reaction mixture was heated at 100 °C for 2 h. The mixture was poured into 1 M $NaHCO_3$. EtOAc was added, and the layers were separated. The organic portion was dried with Na_2SO_4 , filtered, and concentrated. The crude material was purified by silica gel chromatography using 1 \rightarrow 10% (10:1 MeOH/ NH_4OH) in DCM to provide **N**-(6-(3-(2-aminopyrimidin-4-yl)pyridin-2-yloxy)pyridin-3-yl)-4-phenylphthalazin-1-amine (2.1 g, 49% yield) as a light-yellow solid: mp (DSC) 198 °C. 1H NMR (400 MHz, DMSO- d_6) δ ppm 9.48 (1H, s), 8.74 (1H, d, $J = 4.0$ Hz), 8.65 (1H, d, $J = 8.0$ Hz), 8.50 (1H, d, $J = 8.0$ Hz), 8.40 (1H, d, $J = 8.0$ Hz), 8.33–8.29 (2H, m), 8.07 (1H, t, $J = 8.0$ Hz), 7.97 (1H, t, $J = 8.0$ Hz), 7.92–7.90 (1H, m), 7.67–7.66 (2H, m), 7.61–7.55 (3H, m), 7.38–7.35 (1H, m), 7.27–7.23 (2H, m), 6.74 (2H, br s). HRMS m/z $[M + H]^+$ Calcd for $C_{28}H_{20}N_8O$: 485.1833. Found: 485.1834.

N-(4-(3-(2-Aminopyrimidin-4-yl)pyridin-2-yloxy)phenyl)-4-(pyridin-2-yl)phthalazin-1-amine (23e). Applying similar S_NAr conditions as for **23b**, reaction of **22e** and **20a** provided the title compound (108 mg, 62%) as a white solid. 1H NMR (Bruker, 400 MHz, DMSO- d_6) δ ppm 9.43 (s, 1 H), 8.75–8.81 (m, 1 H), 8.66 (t, $J = 7.3$ Hz, 2 H), 8.38 (dd, $J = 7.6, 1.9$ Hz, 1 H), 8.35 (d, $J = 5.2$ Hz, 1 H), 8.24 (s, 1 H), 8.00–8.09 (m, 3 H), 7.95–8.00 (m, 3 H), 7.54 (m, 1 H), 7.27–7.33 (m, 2 H), 7.21 (s, 2 H), 6.76 (br s, 2 H). MS Calcd for $C_{28}H_{20}N_8O$: $[M]^+ = 484$. Found: $[M + H]^+ = 485$.

N-(6-(3-(2-Aminopyrimidin-4-yl)pyridin-2-yloxy)pyridin-3-yl)-4-(pyridin-2-yl)phthalazin-1-amine (23f). Applying similar S_NAr conditions as for **23b**, reaction of **22e** and **20b** followed by silica gel chromatography (0 \rightarrow 100% MeOH in DCM) provided the title compound (92 mg, 53%) as a light-yellow solid. 1H NMR (400 MHz, DMSO- d_6) δ ppm 9.58 (1 H, s), 8.78 (1 H, d, $J = 4.8$ Hz), 8.73 (1 H, d, $J = 2.7$ Hz), 8.61–8.69 (2 H, m), 8.49 (1 H, dd, $J = 8.7, 2.8$ Hz), 8.40 (1 H, dd, $J = 7.6, 2.0$ Hz), 8.26–8.35 (2 H, m), 7.93–8.11 (4 H, m), 7.55 (1 H, ddd, $J = 6.8, 4.8, 2.0$ Hz), 7.37 (1 H, dd, $J = 7.5, 4.7$ Hz), 7.21–7.31 (2 H, m), 6.75 (2 H, s). MS Calcd for $C_{27}H_{19}N_9O$: $[M]^+ = 485$. Found: $[M + H]^+ = 486$.

N-(6-(3-(2-Aminopyrimidin-4-yl)pyridin-2-yloxy)pyridin-3-yl)-4-(5-methylpyridin-2-yl)phthalazin-1-amine (23g). Applying similar S_NAr conditions as for **23b**, reaction of 1-chloro-4-(5-methylpyridin-2-yl)phthalazine (**22g**)³⁵ and **20b** provided the title compound (68 mg, 54%) as a tan solid (94% purity by HPLC). 1H NMR (Bruker, 400 MHz, DMSO- d_6) δ : 9.56 (br s, 1H), 8.73 (m, 1H),

8.68–8.62 (m, 3H), 8.50–8.48 (m, 1H), 8.41 (d, $J = 6.9$ Hz, 1H), 8.33–8.30 (m, 2H), 8.05 (t, $J = 7.7$ Hz, 1H), 7.99–7.95 (m, 2H), 7.86 (d, $J = 8.4$ Hz, 1H), 7.37 (dd, $J = 12, 5$ Hz, 1H), 7.28 (d, $J = 8.6$ Hz, 1H), 7.22 (d, $J = 5$ Hz, 1H), 6.77 (s, 2H), 2.42 (s, 3H). MS Calcd for $C_{28}H_{21}N_9O$: $[M]^+ = 499$. Found: $[M + H]^+ = 500$.

N-(4-(3-(2-Aminopyrimidin-4-yl)pyridin-2-yloxy)phenyl)-4-(5-methylpyridin-2-yl)phthalazin-1-amine (23h). Applying similar S_NAr conditions as for **23b**, reaction of **22g**³⁵ and **20a** provided the title compound (59 mg, 43%) as a white solid. 1H NMR (Bruker, 400 MHz, DMSO- d_6) δ ppm 9.40 (br s, 1 H), 8.63–8.69 (m, 2 H), 8.59–8.62 (m, 1 H), 8.36–8.40 (m, 1 H), 8.35 (d, $J = 5.2$ Hz, 1 H), 8.22–8.25 (m, 1 H), 7.92–8.07 (m, 5 H), 7.81–7.88 (m, 1 H), 7.31 (s, 2 H), 7.20 (d, $J = 8.8$ Hz, 2 H), 6.76 (br s, 2 H), 2.42 (s, 3 H). HRMS m/z $[M + H]^+$ Calcd for $C_{29}H_{22}N_9O$: 499.1989. Found: 499.1993.

N-(6-(3-(2-Aminopyrimidin-4-yl)pyridin-2-yloxy)pyridin-3-yl)-4-(6-methylpyridin-2-yl)phthalazin-1-amine (22i). Applying similar S_NAr conditions as for **23b**, reaction of 1-chloro-4-(6-methylpyridin-2-yl)phthalazine (**22i**)³⁵ and **20b** in *t*-BuOH provided the title compound as a light-yellow solid. 1H NMR (400 MHz, DMSO- d_6) δ ppm 9.56 (1H, s), 8.73 (1H, m), 8.65–8.62 (2H, m), 8.51–8.48 (1H, m), 8.41–8.37 (1H, m), 8.33–8.32 (1H, d, $J = 5.3$ Hz), 8.31–8.29 (1H, m), 8.07–8.03 (1H, m), 8.00–7.96 (1H, m), 7.93–7.89 (1H, t, $J = 7.6, 7.9$), 7.83–7.81 (1H, m), 7.41–7.39 (1H, m), 7.39–7.36 (1H, m), 7.28–7.26 (1H, m), 7.24–7.23 (1H, d, $J = 5.3$ Hz), 6.76 (2H, s), 2.61 (3H, s). HRMS m/z $[M + H]^+$ Calcd for $C_{28}H_{21}N_9O$: 500.1942. Found: 500.1946.

N-(4-(3-(2-Aminopyrimidin-4-yl)pyridin-2-yloxy)phenyl)-4-(6-methylpyridin-2-yl)phthalazin-1-amine (23j). Applying similar S_NAr conditions as for **23b**, reaction of **22i** and **20a** in butan-2-ol followed by reverse-phase chromatography (10–90% 0.1% TFA/ACN in 0.1% TFA/water), neutralization by extraction with DCM and saturated aq $NaHCO_3$, and trituration in EtOH provided the title compound (200 mg, 27% yield); mp (DSC) 235 °C. 1H NMR (400 MHz, DMSO- d_6) δ ppm 9.25 (1H, s), 8.49–8.52 (2H, t, $J = 3.0, 7.3$), 8.20–8.25 (2H, m), 8.08–8.09 (1H, m), 7.74–7.90 (5H, m), 7.37–7.69 (1H, d, $J = 7.5$), 7.24–7.26 (1H, d, $J = 7.4$), 7.14–7.17 (2H, m), 7.07–7.13 (2H, d, $J = 9$), 6.60 (2H, s), 2.46 (3H, s). HRMS m/z $[M + H]^+$ Calcd for $C_{29}H_{22}N_8O$: 499.1989. Found: 499.1987.

N-(4-(3-(2-Aminopyrimidin-4-yl)pyridin-2-yloxy)phenyl)-4-(4-fluorophenyl)phthalazin-1-amine (23k). To a 20 mL microwave tube, **23b** (123 mg, 278 μ mol), 4-fluorophenylboronic acid (58 mg, 420 μ mol), 1.0 M aq CS_2CO_3 solution (560 μ L, 560 μ mol), and THF (0.6 mL) were added. The vessel was purged with nitrogen and sealed, and the mixture was stirred while heating to 160 °C by microwave for 10 min. The mixture was diluted with EtOAc, and the organic layer was washed with water and brine, dried with Na_2SO_4 , and concentrated. Purification by silica gel chromatography (0–10% MeOH in DCM) followed by trituration with EtOH provided the title compound (47 mg, 34% yield) as a light-yellow solid; mp (DSC) 237 °C and 246 °C (multiple polymorphs). 1H NMR (400 MHz, DMSO- d_6) δ ppm 9.34 (1H, s), 8.69–8.67 (1H, d, $J = 8.8$ Hz), 8.39–8.34 (2H, m), 8.24–8.23 (1H, m), 8.07–8.03 (1H, m), 7.98–7.96 (2H, d, $J = 8.8$ Hz), 7.98–7.93 (1H, m), 7.89–7.87 (1H, d, $J = 8.1$ Hz), 7.74–7.70 (2H, m), 7.43–7.39 (2H, t, $J = 8.8$), 7.32–7.27 (2H, m), 7.20–7.18 (2H, d, $J = 9.1$), 6.74 (2H, s). HRMS m/z $[M + H]^+$ Calcd for $C_{29}H_{20}FN_7O$: 502.1786. Found: 502.1785.

N-(4-(3-(2-Aminopyrimidin-4-yl)pyridin-2-yloxy)phenyl)-4-(4-chlorophenyl)phthalazin-1-amine (23l). Applying similar S_NAr conditions as for **23b**, reaction of 1-chloro-4-(4-chlorophenyl)-phthalazine (**22l**)³⁵ and **20a** in butan-2-ol provided the title compound (349 mg, 93% yield) as an off-white solid. 1H NMR (400 MHz, DMSO- d_6) δ ppm 9.34 (s, 1H), 8.68 (d, $J = 8.22$ Hz, 1H), 8.32–8.43 (m, 2H), 8.23 (dd, $J = 2.05, 4.79$ Hz, 1H), 8.01–8.09 (m, 1H), 7.92–8.01 (m, 3H), 7.85–7.90 (m, 1H), 7.68–7.74 (m, 2H), 7.60–7.66 (m, 2H), 7.26–7.33 (m, 2H), 7.16–7.22 (m, 2H), 6.71 (s, 2H). HRMS m/z $[M + H]^+$ Calcd for $C_{29}H_{20}ClN_7O$: 518.1491. Found: 518.1488.

N-(4-(3-(2-Aminopyrimidin-4-yl)pyridin-2-yloxy)phenyl)-4-(3-chlorophenyl)phthalazin-1-amine (23m). Applying similar S_NAr conditions as for **23b**, reaction of **22m** and **20a** in butan-2-ol provided the title compound (146 mg, 78% yield) as an off-white solid.

¹H NMR (400 MHz, DMSO-*d*₆) δ 9.36 (s, 1H), 8.69 (d, *J* = 8.02 Hz, 1H), 8.32–8.42 (m, 2H), 8.23 (dd, *J* = 2.01, 4.84 Hz, 1H), 8.02–8.10 (m, 1H), 7.93–8.01 (m, 3H), 7.88 (d, *J* = 8.12 Hz, 1H), 7.72 (s, 1H), 7.57–7.68 (m, 3H), 7.25–7.33 (m, 2H), 7.19 (d, *J* = 9.00 Hz, 2H), 6.71 (s, 2H). HRMS *m/z* [M + H]⁺ Calcd for C₂₉H₂₀ClN₇O: 518.1491. Found: 518.1500.

N-(4-(3-(2-Aminopyrimidin-4-yl)pyridin-2-yloxy)phenyl)-4-(benzo[d][1,3]dioxol-5-yl)phthalazin-1-amine (23n). Applying similar S_NAr conditions as for 23b, reaction of 22n and 20a in *t*-BuOH provided the title compound (120 mg, 81%) as off-white solid. ¹H NMR (400 MHz, DMSO-*d*₆) δ ppm 9.29 (1H, s), 8.66–8.64 (1H, d, *J* = 8.2 Hz), 8.39–8.37 (1H, m), 8.35–8.34 (1H, d, *J* = 5.3 Hz), 8.24–8.22 (1H, m), 8.04–8.01 (1H, m), 7.97–7.93 (4H, m), 7.32–7.30 (1H, d, *J* = 5.3 Hz), 7.30–7.27 (1H, m), 7.22–7.17 (3H, m), 7.14–7.12 (1H, d, *J* = 8.2 Hz), 7.12–7.09 (1H, m), 6.74 (2H, s), 6.14 (2H, s). HRMS *m/z* [M + H]⁺ Calcd for C₃₀H₂₁N₇O₃: 528.1779. Found: 528.1784.

N-(4-(3-(2-Aminopyrimidin-4-yl)pyridin-2-yloxy)phenyl)-4-(thiophen-2-yl)phthalazin-1-amine (23o). Applying similar S_NAr conditions as for 23b, reaction of 22o and 20a in *t*-BuOH provided the title compound (71 mg, 49%) as a white solid. ¹H NMR (Bruker, 400 MHz, DMSO-*d*₆) δ ppm 9.32 (s, 1 H), 8.66 (d, *J* = 8.3 Hz, 1 H), 8.38 (dd, *J* = 7.6, 1.9 Hz, 1 H), 8.35 (d, *J* = 5.2 Hz, 1 H), 8.23 (m, *J* = 4.7, 2.0 Hz, 1 H), 8.11–8.15 (m, 1 H), 7.94–8.08 (m, 5 H), 7.74–7.79 (m, 1 H), 7.54 (dd, *J* = 4.9, 1.1 Hz, 1 H), 7.26–7.33 (m, 2 H), 7.17–7.21 (m, 2 H), 6.74 (s, 2 H). HRMS *m/z* [M + H]⁺ Calcd for C₂₇H₁₉N₇OS: 490.1445. Found: 490.1445.

N-(4-(3-(2-Aminopyrimidin-4-yl)pyridin-2-yloxy)phenyl)-4-(thiophen-2-yl)phthalazin-1-amine (23p). In a 10 mL pressure-resistant vessel, 23b (90 mg, 204 μmol), Pd(dppf)Cl₂ (30 mg, 41 μmol), and thiophen-2-ylboronic acid (78 mg, 611 μmol) were added. The vessel was purged with argon, and 1,4-dioxane (1 mL) and 2 M aq Na₂CO₃ solution (0.22 mL, 45 μmol) was added. The resulting mixture was stirred at 100 °C for 1.5 h. After cooling to rt, the mixture was diluted with EtOAc and washed with saturated NaHCO₃. The organic layer was dried over Na₂CO₃, concentrated, and purified by reverse-phase chromatography (10–90% 0.1% TFA/ACN in 0.1% TFA/water) to afford the title compound (30 mg, 30% yield) as a white solid; mp (DSC) 258 °C. ¹H NMR (Bruker, 400 MHz, DMSO-*d*₆) δ ppm 9.38 (s, 1 H) 8.68 (d, *J* = 7.7 Hz, 1 H) 8.34–8.42 (m, 3 H) 8.23 (dd, *J* = 4.8, 1.9 Hz, 1 H) 7.99–8.12 (m, 2 H) 7.92–7.97 (m, 2 H) 7.75 (dd, *J* = 5.1, 0.8 Hz, 1 H) 7.68–7.70 (m, 1 H) 7.27–7.32 (m, 3 H) 7.17–7.22 (m, 2 H) 6.74 (s, 2 H). HRMS *m/z* [M + H]⁺ Calcd for C₂₇H₁₉N₇OS: 490.1445. Found: 490.1449.

N-(4-(3-(2-Aminopyrimidin-4-yl)pyridin-2-yloxy)phenyl)-4-(5-methylthiophen-2-yl)phthalazin-1-amine (23q). Applying similar Suzuki coupling conditions as for 23p, reaction of 23b and 5-methylthiophen-2-ylboronic acid provided the title compound (15 mg, 10%) as a white solid. ¹H NMR (400 MHz, DMSO-*d*₆) δ ppm 9.34 (br s, 1 H) 8.66 (d, *J* = 8.0 Hz, 1 H) 8.32–8.46 (m, 3 H) 8.20–8.26 (m, 1 H) 7.98–8.10 (m, 2 H) 7.94 (d, *J* = 8.6 Hz, 2 H) 7.46–7.50 (m, 1 H) 7.25–7.36 (m, 2 H) 7.19 (d, *J* = 8.1 Hz, 2 H) 6.94–7.01 (m, 1 H) 6.74 (br s, 2 H) 2.54 (br s, 3 H). HRMS *m/z* [M + H]⁺ Calcd for C₂₈H₂₁N₇OS: 504.1601. Found: 504.1608.

N-(4-(3-(2-Aminopyrimidin-4-yl)pyridin-2-yloxy)phenyl)-4-(4-methylthiophen-2-yl)phthalazin-1-amine (23r). Applying similar S_NAr conditions as for 23b, reaction of 22r and 20a in 2-butanol provided the title compound (2.08 g, 49%) as an off-white solid; mp (DSC) 216 °C. ¹H NMR (400 MHz, DMSO-*d*₆) δ ppm 9.36 (s, 1 H) 8.64–8.69 (m, 1 H) 8.41–8.44 (m, 1 H) 8.36–8.40 (m, 1 H) 8.35 (d, *J* = 5.2 Hz, 1 H) 8.23 (dd, *J* = 4.8, 2.0 Hz, 1 H) 8.00–8.10 (m, 2 H) 7.91–7.97 (m, 2 H) 7.52 (d, *J* = 1.0 Hz, 1 H) 7.26–7.33 (m, 3 H) 7.16–7.22 (m, 2 H) 6.74 (br s, 2 H) 2.34 (br s, 3 H). ¹³C NMR (150 MHz, DMSO-*d*₆) δ 163.81, 160.72, 160.67, 158.68, 151.64, 148.50, 148.36, 147.14, 139.86, 139.24, 137.72, 137.10, 132.61, 131.74, 130.24, 125.27, 124.89, 122.92, 122.83, 122.44, 121.56, 121.52, 119.11, 118.23, 109.93, 15.6 HRMS *m/z* [M + H]⁺ Calcd for C₂₈H₂₁N₇OS: 504.1601. Found: 504.1607.

N-(4-Iodophenyl)-4-phenylphthalazin-1-amine Hydrochloride (25). 4-Iodobenzenamine (0.910 g, 4.15 mmol) and 1-chloro-4-

phenylphthalazine (1.00 g, 4.15 mmol) were suspended in 20 mL of butan-2-ol and heated to 110 °C in a sealed tube overnight. The light-yellow slurry was cooled and filtered, rinsed with 2-PrOH, and dried in vacuo to give *N*-(4-iodophenyl)-4-phenylphthalazin-1-amine hydrochloride (1.69 g, 88%) as a light-yellow solid. ¹H NMR (400 MHz, DMSO-*d*₆) δ ppm 10.84 (1 H, br s), 8.98 (1 H, d, *J* = 8.1 Hz), 8.28 (1 H, t, *J* = 7.8 Hz), 8.17 (1 H, t, *J* = 7.7 Hz), 8.01 (1 H, d, *J* = 7.8 Hz), 7.82–7.91 (2 H, m), 7.64–7.76 (5 H, m), 7.57–7.63 (2 H, m). MS (ESI) *m/z* Calcd for C₂₀H₁₄IN₃: [M]⁺ = 423. Found: [M + H]⁺ = 424.

6-(4-(4-Phenylphthalazin-1-ylamino)phenyl)quinazolin-2-amine (27). 6-(4,4,5,5-Tetramethyl-1,3,2-dioxaborolan-2-yl)-quinazolin-2-amine³³ (0.1 g, 0.5 mmol), *N*-(4-iodophenyl)-4-phenylphthalazin-1-amine hydrochloride (0.200 g, 0.4 mmol), and Pd(dppf)Cl₂ (0.02 g, 0.02 mmol) were combined in 2 mL of 1,4-dioxane and 2 M aq Na₂CO₃ solution (0.7 mL, 1 mmol). The reaction was flushed with nitrogen, sealed, and heated at 90 °C overnight. After cooling, the mixture was diluted in EtOAc/water. The organic layer was dried over Na₂SO₄, filtered, and concentrated. The residue was taken up in DCM/MeOH and adsorbed onto 2 g of silica gel and purified by silica gel chromatography (0–10% MeOH/DCM) to provide the title compound (9 mg, 5% yield). ¹H NMR (400 MHz, DMSO-*d*₆) δ ppm 9.41 (1 H, s), 9.18 (1 H, s), 8.71 (1 H, d, *J* = 8.5 Hz), 8.02–8.19 (5 H, m), 7.87–8.00 (2 H, m), 7.75–7.83 (2 H, m), 7.65–7.72 (2 H, m), 7.53–7.63 (3 H, m), 7.51 (1 H, d, *J* = 8.8 Hz), 6.87 (2 H, s). MS (ESI) *m/z* Calcd for C₂₈H₂₀N₆: [M]⁺ = 440. Found: [M + H]⁺ = 441.

N-(4-((2-Aminopyrimidin-5-yl)ethynyl)phenyl)-4-phenylphthalazin-1-amine (29). Copper(I) iodide, 99.999% (0.0041 g, 0.022 mmol), bis(triphenylphosphine)palladium(II) chloride (0.015 g, 0.022 mmol), 5-ethynylpyrimidin-2-amine³⁴ (0.10 g, 0.87 mmol), and 24 (0.200 g, 0.44 mmol) were combined in a sealed tube and diluted with 5 mL of 3:1 ACN/TEA. The reaction was sealed and heated to 90 °C overnight. The mixture was cooled and adsorbed onto 2 g of silica gel and purified by silica gel chromatography (0–10% MeOH/DCM). The isolated material was sonicated in 2 mL of DCM, filtered, rinsing with DCM, to provide the title compound (0.094 g, 52% yield) as a light-yellow solid. ¹H NMR (400 MHz, DMSO-*d*₆) δ ppm 9.48 (1 H, s), 8.68 (1 H, d, *J* = 8.2 Hz), 8.43 (2 H, s), 8.01–8.14 (3 H, m), 7.87–8.00 (2 H, m), 7.65–7.73 (2 H, m), 7.47–7.64 (5 H, m), 7.09 (2 H, s). MS (ESI) *m/z* Calcd for C₂₆H₁₈N₆: [M]⁺ = 414. Found: [M + H]⁺ = 415.

2-(Dimethylamino)-3-hydroxy-3-(pyridin-2-yl)isoindolin-1-one (31e). Following the published procedure³⁵ to prepare 2-(dimethylamino)-3-hydroxy-3-(6-methylpyridin-2-yl)isoindolin-1-one, reaction of 2-bromopyridine (1.2 mL, 13 mmol), *n*-BuLi (5.3 mL, 13 mmol; 2.5 M solution in THF), and 2-(dimethylamino)isoindoline-1,3-dione (2.9 g, 15 mmol) provided the title compound as a light-orange solid (2.2 g, 65%). ¹H NMR (400 MHz, DMSO-*d*₆) δ 8.40–8.39 (m, 1H), 7.95–7.93 (m, 1H), 7.90–7.86 (m, 1H), 7.67–7.65 (m, 1H), 7.54–7.47 (m, 2H), 7.32–7.29 (m, 1H), 7.15 (s, 1H), 7.14–7.13 (m, 1H), 2.71 (s, 6H). HRMS Calcd for C₁₅H₁₅N₃O₂: [M + H]⁺ = 270.1237, [M + Na]⁺ = 292.1057. Found: [M + H]⁺ = 270.1245, [M + Na]⁺ = 292.1059.

4-(Pyridin-2-yl)phthalazin-1(2H)-one (31e). Following the published procedure to prepare 4-(6-methylpyridin-2-yl)phthalazin-1(2H)-one,³⁵ reaction of 2-(dimethylamino)-3-hydroxy-3-(pyridin-2-yl)isoindolin-1-one 31e (2.00g, 7.43 mmol) and hydrazine (3.50 mL, 111 mmol) provided the title compound as an off-white solid (1.34g, 80.8% yield). ¹H NMR (400 MHz, DMSO-*d*₆) δ 12.56 (s, 1H), 8.75–8.74 (m, 1H), 8.39–8.37 (m, 1H), 8.34–8.32 (m, 1H), 8.02–7.98 (m, 1H), 7.92–7.84 (m, 3H), 7.55–7.52 (m, 1H). HRMS Calcd for C₁₃H₉N₃O: [M + H]⁺ = 224.0818, [M + Na]⁺ = 246.0638. Found: [M + H]⁺ = 224.0820, [M + Na]⁺ = 246.0642.

Homogenous Time-Resolved Fluorescence Enzyme Assays. IC₅₀ values for the inhibition of the AurA/TPX2 complex, AurB, and other kinase enzymes were measured using an HTRF assay as described.⁶

Transport across MDR1-LLC-PK1 Cells. Transport studies to determine apparent permeability and efflux ratios [Efflux ratio = *P*_{appB→A}/*P*_{appA→B}] were performed in MDR1-transfected LLC-PK1

cells with compounds tested at 5 μ M in the presence of 0.1% BSA as described.⁵⁶

Plasma Protein Binding. Data were obtained in duplicate by equilibrium dialysis.¹⁴

Rat and Human Liver Microsomal Assays. Test compounds (1 μ M) were incubated at 37 °C in phosphate buffer (66.7 mM, pH 7.4) with pooled human or rat liver microsomes (0.25 mg/mL protein) and 1 mM NADPH. After 30 min, the reaction was stopped by the addition of acetonitrile containing 0.5% formic acid and internal standard. The quenched samples were centrifuged at 1650g for 20 min. The supernatants were analyzed directly for unchanged test compound using liquid chromatography and tandem mass spectrometric detection (LC-MS/MS).

CYP3A4 Inhibition IC₅₀ Shift. Inhibition of CYP3A4 by **23n** was determined by measuring the conversion of midazolam to 1-hydroxymidazolam by human microsomal protein in the presence of a 7-point range of **23n** conc that were added simultaneously with the midazolam or 30 min prior.⁵⁷

Solubility Determination. Solubilities in 0.01 N HCl and PBS were determined according to an automated procedure.⁴⁴

Pharmacokinetic Studies. Male Sprague–Dawley rats with surgically implanted femoral vein and jugular vein cannulae were dosed as described.⁶ Oral doses were formulated in either OraPlus, pH 2.2, or 2% HPMC/1% Tween 80 in water, pH 2.2, as indicated in Tables 3 and 4. Intravenous doses were formulated in DMSO except in the case of **23d** and **23r**, which were formulated in 10% EtOH/20% propylene glycol/20% polyethylene glycol 400 in water.

Cell Lines and Cellular Assays. Human cancer cell lines were obtained from the American Type Culture Collection (ATCC) and grown under recommended conditions unless otherwise specified. CAL51 breast cancer cell line was obtained from Deutsche Sammlung von Mikroorganismen und Zellkulturen (Brunswick, Germany). Cells were fixed with fixation buffer (3.7% formaldehyde and 0.1% glutaraldehyde in PBS) unless otherwise specified. Washing and staining steps were performed in wash buffer (0.2% Triton X-100 and 1% BSA in PBS) unless otherwise specified. All high-content imaging assays were performed on an ArrayScan VTI HCS reader (Cellomics, Thermo Fisher Scientific). All flow cytometry assays were performed on a LSRII flow cytometer running FACSDiva software (BD Biosciences Immunocytometry Systems).

HeLa DNA Ploidy Assay. EC₅₀ values for generation of $\geq 4N$ DNA-content in HeLa cells were determined in duplicate by high-content cell imaging.⁶

p-HH3 Assay (Imaging, 24 h). MES-SA and MES-SADx5 (doxorubicin-resistant) cells were plated at a density of 1000 cells per well in a 96-well plate in complete media (McCoy's 5A/1 \times glutamine, 10% FBS). The following day, cells were treated with DMSO or AKI compounds over an 11-point concentration range that was based on compound potency (assay run in duplicate). After 24 h, cells were fixed in fixation buffer for 10 min at room temperature. Cells were then permeabilized with wash buffer and immunostained with an anti-p-HH3 serine-10 antibody (Millipore). Next, the cells were washed with wash buffer, and secondary detection was performed by incubating the cells with an anti-rabbit IgG-Alexa-568 antibody (Invitrogen) and Hoechst 33342 DNA dye for 30 min at rt. Cell assay plates were washed twice with wash buffer and analyzed using Target Activation V2 algorithm (Cellomics). The percentage of p-HH3 positive cells was determined and used to generate concentration–response curves and IC₅₀ values fitted by a four-parameter equation.

Cell Count Assay (Imaging, 72 h). Cancer cell lines (CAL51, HCT-15, MES-SADx5, SNU449, and 769P) were plated at a density of 3000 or 5000 cells per well (depending on the cell line growth kinetics) in a 96-well plate in complete growth media. The following day, cells were treated with DMSO or AKI compounds over an 11-point concentration range that was based on compound potency (assay run in duplicate). After 24 h, the growth media containing compound was removed and the cells were washed once with media alone. Cells were then incubated in fresh growth media (without compound) for an additional 48 h. Cells were fixed in fixation buffer

for 10 min at rt. Cells were permeabilized with wash buffer and stained with Hoechst 33342 DNA dye for 30 min at rt. Next, the cells were washed once with wash buffer and analyzed using a Morphology V2 algorithm (Cellomics). A threshold based on nuclei size was set using the DMSO-control (normal nuclear size range was equal to mean nuclear area plus one standard deviation). The percentage of normal size nuclei was determined and used to generate concentration–response curves and IC₅₀ values fitted by a four-parameter equation.

Cross-Species Serum Shift of p-HH3 Inhibition in Jurkat Cells Treated with **23r in the presence of 5% and 25% serum.**

23r was preincubated for 1 h in complete media (RPMI 1640/1 \times glutamine supplemented with 5% and 25% serum from mouse, rat, dog, or monkey) over an 11-point concentration range (0.0029–3 μ M) with a final DMSO concentration of 0.1% in media. Next, Jurkat cells were treated with compound plus complete media at a density of 2.5×10^5 cells per tube and incubated for 3 h at 37 °C with 5% CO₂. After 3 h, cells were centrifuged and washed twice with 200 μ L of cold 1 \times PBS. After the last wash and centrifugation, the cells were fixed in 200 μ L of ice cold 90% MeOH and stored at –20 °C overnight. The following day, cells were centrifuged and washed with 200 μ L of wash buffer. Cells were stained with anti-p-HH3-Alexa-488 antibody (1 μ g/mL) and counterstained with Hoechst 33342 nuclear dye for 1.5 h at rt in the dark. After the incubation the cells were centrifuged and washed with 200 μ L of wash buffer and resuspended into 100 μ L of wash buffer and transferred to a 96-well PackardView plate. The plate was then centrifuged at 2000 rpm to displace cells to the bottom of the wells. The p-HH3 signal was then analyzed and quantified using ArrayScan VTI TargetActivation.V2 Bioapplication. These data were used to generate concentration–response curves and IC₅₀ values fitted by a four-parameter equation.

p-HH3 Assay (Imaging, Time Course). Jurkat cells were plated at a density of 2.0×10^5 cells per well in a 96-well plate in complete media (RPMI 1640/1 \times glutamine, 10% FBS). Cells were treated with DMSO or **23r** over an 11-point concentration range that was based on the time point: 1 and 3 h time points had a top dose of 1000 nM; 8 and 24 h time points, top dose of 125 nM. Cells were incubated with **23r** for 1, 3, 8, and 24 h and then fixed with ice-cold 90% MeOH for 24 h at 20 °C. Cells were permeabilized with wash buffer and immunostained with an anti-p-HH3 serine-10-Alexa-488 antibody (Cell Signaling) for 2 h at rt in the dark. Cells were washed and counterstained with 4',6-diamidino-2-phenylindole (DAPI, Invitrogen) DNA dye for 30 min at rt. Cells were washed twice with wash buffer and allowed to sit overnight at 4 °C before being analyzed using Target Activation V2 algorithm (Cellomics). The percentage of p-HH3 positive cells was determined and used to generate concentration–response curves and IC₅₀ values fitted by a four-parameter equation.

p-AurA and p-HH3 Assay (Imaging, 6 h). HCT-116 and HeLa cells were treated with 2 mM thymidine for 16 h to semisynchronize the cells in G₁-S phase of the cell cycle. Two and three h after a G₁-S release, cells were treated with **23r** compound (concentration range 0.3–156 nM, assay repeated in two independent experiments) in complete growth media (HCT-116, McCoy's 5A/1 \times glutamine, 10% FBS; HeLa, DMEM/1 \times glutamine, 10% FBS, 1 \times NEAA) for an additional 6 h to enrich for mitotic cells. Cells were fixed in 3.7% formaldehyde for 15 min at rt, followed by treatment and storage in ice-cold 90% MeOH. Cells were permeabilized with wash buffer and immunostained with either anti-p-HH3 serine-10 (Millipore), or anti-p-AurA threonine-288 (Cell Signaling) antibodies. Secondary detection was performed by incubating the cells with an anti-rabbit IgG-Alexa-568 antibody and DAPI for 30 min at rt. Individual mitotic objects were segmented as the primary mask, and the mean fluorescence intensity was determined for p-HH3 and p-AurA regions using Compartmental Analysis V2 algorithm (Cellomics). DMSO-treated cells served as a baseline control for p-HH3 and p-AurA fluorescence intensity and used to generate concentration–response curves and EC₅₀ values fitted by a four-parameter equation.

AKI Washout p-HH3 Assay (Flow Cytometry). Jurkat cells in complete media (RPMI 1640/1 \times glutamine, 10% FBS) were treated for 3 h with DMSO or AKI compounds [**23r** (250 nM), **1** (500 nM),

3b (250 nM), and **2** (1000 nM); assay repeated in two independent experiments]. Cells were then centrifuged and washed twice with media alone to remove any remaining AKI compound. Cells (2.0×10^5 cells per time point) were then cultured in complete media and harvested at 0, 10, 30, and 45 min and 1, 2, 4, 6, 10, and 24 h. Cells were fixed with ice-cold 90% MeOH for 24 h at -20°C . Cells were permeabilized with wash buffer and immunostained with an anti-p-HH3 serine-10 antibody (Millipore). Secondary detection was performed by incubating cells with an anti-rabbit IgG-Alexa-647 antibody and propidium iodide (PI) supplemented with RNase I (BD Biosciences) for 30 min at rt. Data was analyzed by flow cytometry. A threshold gate was applied according to DNA content and p-HH3 positive 4N cell population. The percentage of p-HH3+ events was determined for each AKI compound and each time interval. DMSO-treated controls were analyzed at 1 and 24 h time points.

Biosensor Binding Assays. AurB was immobilized on a CMS sensor surface on the Biacore T200 system using standard amine coupling chemistry resulting in a surface density of approximately 1000 RU. The sensor surface was washed with 10 separate injections of running buffer (50 mM HEPES pH7.4, 5 mM NaCl, 0.5 mM MgCl, 0.5 mM MnCl, and 2.5% DMSO) for 60 s. Compound was tested using a 3-fold dilution series starting at 1 mM using a single site kinetics method. Data were collected at 25°C . Sensor data were processed using Biacore T200 Evaluation software (GE Healthcare Life Sciences) and fit to a 1:1 model.

Mouse Studies. Female athymic nude mice (Harlan Sprague–Dawley) of approximately 9 weeks of age were housed five per filter-capped cage. All animal studies were performed under pathogen-free conditions in facilities approved by the American Association of Laboratory Animal Care and in accordance with current regulations and standards of the U.S. Department of Agriculture and the National Institutes of Health. Animals were fed a commercial rodent chow and received filter-purified tap water ad libitum. During the HCT-116 tumor xenograft efficacy study, animals also received transgel (Charles River), cherry nutragel (Bioserve), and nutrical (Evsco) as dietary supplements placed on the floor of the cage the entire course of the treatment phase.

Mouse Bone Marrow PK–PD. Mice were administered a single oral dose (PO) of **23c** and **23r** AKI compounds at 3, 10, and 30 mg/kg or vehicle alone ($n = 3$ animals per group). Six hours after treatment, mice were sacrificed and plasma (for pharmacokinetic analysis) and bone marrow were collected. To isolate mouse bone marrow (BM) cells, femur bone were flushed with 1 mL of BM harvest buffer (1× HBSS (Invitrogen), 1% BSA) using 1 mL syringe, and cells were centrifuged and fixed with ice-cold 90% MeOH for 24 h at -20°C . Bone marrow cells ($\sim 1 \times 10^6$ cells per tube) were permeabilized with wash buffer and then incubated with acid buffer (2 N HCl, 0.5% Triton X-100 in distilled water) for 45 min at rt. Cells were washed thrice in wash buffer. Next, cells were immunostained with anti-p-HH3 serine-10 antibody (Millipore) for 90 min at rt. Secondary detection was performed by incubating cells with an anti-rabbit IgG-Alexa-647 antibody (Invitrogen) for 45 min at rt in the dark. Stained cells were centrifuged, washed, and counterstained with PI supplemented with RNase I for 30 min at rt in the dark. Cells were filtered through 35 μm cell strainer and transferred into 5 mL FACS tubes (Falcon). Data was analyzed by flow cytometry. The primary gating strategy was based on DNA content (double discrimination) and threshold gates applied to the detectable G2/M cell population (4N DNA content) and its corresponding p-HH3 subpopulation. Bone marrow from mice treated with the vehicle served as the p-HH3 staining control. The total percentage of G2/M and p-HH3 positive cells in G2/M was determined for each bone marrow sample and plotted versus plasma concentration of AKI compound.

COLO205 Tumor Xenograft PK–PD. Mice were implanted with 2×10^6 COLO205 cells subcutaneously on the right flank. Mice with established tumors ($\sim 200\text{ mm}^3$) were assigned into one of six groups ($n = 6$ per group). A single oral dose was administered to each group: vehicle alone or **23r** at 1.5, 3.5, 7.5, 15, and 30 mg/kg. Three or six hours after treatment ($n = 3$ per group per time point), mice were sacrificed and the following specimens were collected: blood (for

plasma PK analysis), bone marrow, and tumor. Bone marrow specimens were processed for p-HH3 immunostaining as described above. Excised tumors were immediately minced into fine pieces with a razor blade and transferred into 10 mL of cell dissociation buffer [1× HBSS, 0.1 mg/mL Collagenase V (Sigma), 0.25 mg/mL Collagenase XI (Sigma), 1% Dispase II (Sigma), and 25 units/mL RNase free DNase I (Roche)] in a 50 mL conical tube with a small magnetic stir bar. Tubes were inverted and placed on a magnetic stir plate and incubated at 37°C for 15 min with constant stirring to facilitate cell dissociation. Cells were passed through a 70 μm filter, centrifuged at 2000 rpm for 4 min, washed in 1 mL of Versene (Invitrogen), and then fixed in ice-cold 90% MeOH for 24 h at -20°C . Fixed cells ($\sim 1 \times 10^6$ cells per tube) were centrifuged and washed once with wash buffer. Next, cells were immunostained with anti-p-HH3 serine-10 antibody (Millipore) and anti-cytokeratin (8/18)-FITC antibody (Clone 5D3, Vector Laboratories) for 90 min at rt in the dark. Secondary detection was performed by incubating cells with an anti-rabbit IgG-Alexa-647 antibody for 45 min at rt in the dark. Cells were washed and counterstained with PI (supplemented with RNase I) for 30 min at rt in the dark. Cells were filtered through 35 μm cell strainer and transferred into 5 mL FACS tubes. Data was analyzed by flow cytometry. The primary gating strategy was based on DNA content (double discrimination) and a nested gate based on cytokeratin fluorescence intensity. Threshold gates were applied to the detectable G2/M cell population (4N DNA content) and its corresponding p-HH3 subpopulation. The total percentage of p-HH3+ events in G2/M was determined for each tumor sample. Tumors from mice treated with vehicle served as p-HH3 staining controls. The total percentage of p-HH3 positive cells in G2/M was plotted against the **23r** plasma concentration for each individual animal (includes vehicle-control group) and used to generate a concentration–response curve and IC_{50} value fitted by a four-parameter equation.

Growth Inhibition of HCT-116 Tumor Xenografts in Vivo.

Mice were implanted with 2×10^6 cells (100 μL) subcutaneously on their right flank. After 7 days, tumor-bearing mice were measured and randomized into groups ($n = 10$ each). Treatment began on day 8, with groups that included: vehicle (2% HPMC/1% Tween 80 in water, pH 2.2), BID, PO 7 days per week; **23r** 3 mg/kg BID, PO 7 days per week; **23r** 60 mg/kg QD, PO days 1 and 4 per week; and 15 mg/kg BID, PO (2 days on then 5 days off per week). An observer blinded to the dosing regimen measured the tumors with a digital caliper and weighed the mice twice per week. Tumor volumes were calculated as follows: tumor volume (mm^3) = $[(W^2 \times L)/2]$ where width (W) is defined as the smaller of the 2 measurements and length (L) is defined as the larger of the 2 measurements. On day 28, after three cycles of treatment, the tumor volume measurement phase was concluded. Whole blood for PK analysis was collected during a fourth dosing cycle. Mice were dosed in the morning, and whole blood for pharmacokinetics analysis was collected at 1, 3, 6, 8, and 24 h ($n = 2$ /time point). Mice on BID treatment and scheduled for the 24 h time point were given a second dose in the evening of blood collection, 8 h after the morning dose, and 16 h prior to the final time point collect. For the 15 mg/kg BID (2 days on/5 days off), group blood collection began on the second day of the dosing cycle. Complete blood counts were collected only at the 1, 3, and 6 h time points for all groups. All tumors were collected and weighed. Data was statistically analyzed with repeated measure ANOVA for tumor volumes over time using Stat View software v5.0.1. Scheffe's posthoc test was used to determine p -values for repeated measures from day 7 to day 28.

■ ASSOCIATED CONTENT

Supporting Information

AKI enzyme and cellular data with statistical information, tabulated mouse bone marrow PK/PD data for **14b**, **23c**, **22k**, and **23r**, and Ambit single point kinase binding data for **23r**. The Supporting Information is available free of charge on the ACS Publications website at DOI: 10.1021/acs.jmedchem.5b00183.

AUTHOR INFORMATION

Corresponding Author

*Phone: 617-444-5041. E-mail: MeyerS@amgen.com.

Present Addresses

[#]For B.D.: Mersana Therapeutics, 840 Memorial Drive, Cambridge, Massachusetts 02139, United States.

[∇]For B.L.H.: Blueprint Medicines, 215 First Street, Cambridge, Massachusetts 02142, United States.

[○]For H.N.N.: Coferon, Inc., 25 Health Sciences Drive, Stony Brook, New York 11790, United States.

[@]For A.B.: Merck & Co., Inc., 1 Merck Drive, Whitehouse Station, New Jersey 08889, United States.

[†]For Y.D.: Alexion Pharmaceuticals, 55 Cambridge Parkway, Cambridge, Massachusetts 02142, United States.

⁺For T.L.B. and R.R.: Janssen Research & Development, LLC, 1400 McKean Road, Spring House, Pennsylvania 19002, United States.

[⊗]For V.F.P.: Sanofi, 153 S Avenue, Waltham, Massachusetts 02451, United States.

Author Contributions

The manuscript was written through contributions of all authors. All authors have given approval to the final version of the manuscript.

Notes

The authors declare the following competing financial interest(s): The authors declare financial interests as current or former Amgen employees and shareholders.

ACKNOWLEDGMENTS

We thank Steve Coats for early project leadership, Paul Reider, Mark Duggan, Sasha Kamb, Graham Molineux, and Glenn Begley for their guidance, Loren Berry for protein binding and CYP inhibition studies, Brett Janofsky for permeability determinations, and Ji-Rong Sun for pharmacology support.

DEDICATION

◇We dedicate this article to the memory of Beth Ziegler, a friend and highly valued colleague who contributed significantly to the progression of 23r from discovery to clinical development. We are thankful for Beth's scientific diligence and commitment to cancer research as a member of the 23r team and multiple other programs at Amgen.

ABBREVIATIONS USED

ACN, acetonitrile; AK, Aurora kinase; AKI, Aurora kinase inhibitor; AurA, Aurora kinase A; AurB, Aurora kinase B; CI, confidence interval; CL, clearance; EtOH, ethanol; G2/M, Gap 2/mitosis; HLM, human liver microsomal; RLM, rat liver microsomal; HPMC, hydroxypropylmethylcellulose; inh, inhibition; MeOH, methanol; P_{app} , apparent permeability; Pd(dppf)Cl₂, 1,1'-bis(diphenylphosphino)ferrocene]-dichloropalladium(II); p-AurA, p-Aurora-A Thr²⁸⁸; p-HH3, phospho-histone H3; SAC, spindle assembly checkpoint; TEA, triethylamine

REFERENCES

- (1) Lens, S. M.; Voest, E. E.; Medema, R. H. Shared and separate functions of polo-like kinases and Aurora kinases in cancer. *Nature Rev. Cancer* **2010**, *10*, 825–841.
- (2) (a) Pollard, J. R.; Mortimore, M. Discovery and development of Aurora kinase inhibitors as anticancer agents. *J. Med. Chem.* **2009**, *52*, 2629–2651. (b) Perez Fidalgo, J. A.; Roda, D.; Rosello, S.; Rodriguez-

Braun, E.; Cervantes, A. Aurora kinase inhibitors: a new class of drugs targeting the regulatory mitotic system. *Clin. Transl. Oncol.* **2009**, *11*, 787–798. (c) Boss, D. S.; Beijnen, J. H.; Schellens, J. H. Clinical experience with Aurora kinase inhibitors: a review. *Oncologist* **2009**, *14*, 780–793. (d) Kollareddy, M.; Zheleva, D.; Dzubak, P.; Brahmshatriya, P. S.; Lepsik, M.; Hajdich, M. Aurora kinase inhibitors: progress towards the clinic. *Invest. New Drugs* **2012**, *30*, 2411–2432.

(3) Barr, A. R.; Gergely, F. Aurora-A: the maker and breaker of spindle poles. *J. Cell Sci.* **2007**, *120*, 2987–2996.

(4) Ditchfield, C.; Johnson, V. L.; Tighe, A.; Ellston, R.; Haworth, C.; Johnson, T.; Mortlock, A.; Keen, N.; Taylor, S. S. Aurora B couples chromosome alignment with anaphase by targeting BubR1, Mad2, and Cenp-E to kinetochores. *J. Cell Biol.* **2003**, *161*, 267–280.

(5) Yang, H.; Burke, T.; Dempsey, J.; Diaz, B.; Collins, E.; Toth, J.; Beckmann, R.; Ye, X. Mitotic requirement for Aurora A kinase is bypassed in the absence of Aurora B kinase. *FEBS Lett.* **2005**, *579*, 3385–3391.

(6) Cee, V. J.; Schenkel, L. B.; Hodous, B. L.; Deak, H. L.; Nguyen, H. N.; Olivieri, P. R.; Romero, K.; Bak, A.; Be, X.; Bellon, S.; Bush, T. L.; Cheng, A. C.; Chung, G.; Coats, S.; Eden, P. M.; Hanestad, K.; Gallant, P. L.; Gu, Y.; Huang, X.; Kendall, R. L.; Lin, M. H.; Morrison, M. J.; Patel, V. F.; Radinsky, R.; Rose, P. E.; Ross, S.; Sun, J. R.; Tang, J.; Zhao, H.; Payton, M.; Geuns-Meyer, S. D. Discovery of a potent, selective, and orally bioavailable pyridinyl-pyrimidine phthalazine Aurora kinase inhibitor. *J. Med. Chem.* **2010**, *53*, 6368–6377.

(7) Harrington, E. A.; Bebbington, D.; Moore, J.; Rasmussen, R. K.; Ajose-Adeogun, A. O.; Nakayama, T.; Graham, J. A.; Demur, C.; Hercend, T.; Diu-Hercend, A.; Su, M.; Golec, J. M. C.; Miller, K. M. VX-680, a potent and selective small-molecule inhibitor of the Aurora kinases, suppresses tumor growth in vivo. *Nature Med.* **2004**, *10*, 262–267.

(8) Fancelli, D.; Moll, J.; Varasi, M.; Bravo, R.; Artico, R.; Berta, D.; Bindi, S.; Cameron, A.; Candiani, I.; Cappella, P.; Carpinelli, P.; Croci, W.; Forte, B.; Giorgini, M. L.; Klapwijk, J.; Marsiglio, A.; Pesenti, E.; Rocchetti, M.; Roletto, F.; Severino, D.; Soncini, C.; Storici, P.; Tonani, R.; Zugnoni, P.; Vianello, P. 1,4,5,6-Tetrahydropyrrolo[3,4-c]pyrazoles: identification of a potent Aurora kinase inhibitor with a favourable antitumour kinase inhibition profile. *J. Med. Chem.* **2006**, *49*, 7247–7251.

(9) Mortlock, A. A.; Foote, K. M.; Heron, N. M.; Jung, F. H.; Pasquet, G.; Lohmann, J. J.; Warin, N.; Renaud, F.; De Savi, C.; Roberts, N. J.; Johnson, T.; Dousson, C. B.; Hill, G. B.; Perkins, D.; Hatter, G.; Wilkinson, R. W.; Wedge, S. R.; Heaton, S. P.; Odedra, R.; Keen, N. J.; Crafter, C.; Brown, E.; Thompson, K.; Brightwell, S.; Khatri, L.; Brady, M. C.; Kearney, S.; McKillop, D.; Rhead, S.; Parry, T.; Green, S. Discovery, synthesis, and in vivo activity of a new class of pyrazoloquinazolines as selective inhibitors of Aurora B kinase. *J. Med. Chem.* **2007**, *50*, 2213–2224.

(10) Schenone, S.; Bruno, O.; Radi, M.; Botta, M. New insights into small-molecule inhibitors of Bcr-Abl. *Med. Res. Rev.* **2011**, *31*, 1–41.

(11) Diamond, J. R.; Bastos, B. R.; Hansen, R. J.; Gustafson, D. L.; Eckhardt, S. G.; Kwak, E. L.; Pandya, S. S.; Fletcher, G. C.; Pitts, T. M.; Kulikowski, G. N.; Morrow, M.; Arnott, J.; Bray, M. R.; Sidor, C.; Messersmith, W.; Shapiro, G. I. Phase I safety, pharmacokinetic, and pharmacodynamic study of ENMD-2076, a novel angiogenic and Aurora kinase inhibitor, in patients with advanced solid tumors. *Clin. Cancer Res.* **2011**, *17*, 849–860.

(12) Payton, M.; Bush, T. L.; Chung, G.; Ziegler, B.; Eden, P.; McElroy, P.; Ross, S.; Cee, V. J.; Deak, H. L.; Hodous, B. L.; Nguyen, H. N.; Olivieri, P. R.; Romero, K.; Schenkel, L. B.; Bak, A.; Stanton, M.; Dussault, I.; Patel, V. F.; Geuns-Meyer, S.; Radinsky, R.; Kendall, R. L. Preclinical evaluation of AMG 900, a novel potent and highly selective pan-Aurora kinase inhibitor with activity in taxane-resistant tumor cell lines. *Cancer Res.* **2010**, *70*, 9846–9854.

(13) (a) Harker, W. G.; Sikic, B. I. Multidrug (pleiotropic) resistance in doxorubicin-selected variants of the human sarcoma cell line MES-SA. *Cancer Res.* **1985**, *45*, 4091–4096. (b) Wesolowska, O.; Paprocka, M.; Kozlak, J.; Motohashi, N.; Dus, D.; Michalak, K. Human sarcoma

cell lines MES-SA and MES-SA/Dx5 as a model for multidrug resistance modulators screening. *Anticancer Res.* **2005**, *25*, 383–389.

(14) Huang, L.; Be, X.; Berry, L.; Moore, E.; Janosky, B.; Wells, M.; Pan, W. J.; Zhao, Z.; Lin, M. H. In vitro and in vivo pharmacokinetic characterizations of AMG 900, an orally bioavailable small molecule inhibitor of Aurora kinases. *Xenobiotica* **2011**, *41*, 400–408.

(15) Cox, C. D.; Breslin, M. J.; Whitman, D. B.; Coleman, P. J.; Garbaccio, R. M.; Fraley, M. E.; Zrada, M. M.; Buser, C. A.; Walsh, E. S.; Hamilton, K.; Lobell, R. B.; Tao, W.; Abrams, M. T.; South, V. J.; Huber, H. E.; Kohl, N. E.; Hartman, G. D. Kinesin spindle protein (KSP) inhibitors. Part V: discovery of 2-propylamino-2,4-diaryl-2,5-dihydropyrroles as potent, water-soluble KSP inhibitors, and modulation of their basicity by beta-fluorination to overcome cellular efflux by P-glycoprotein. *Bioorg. Med. Chem. Lett.* **2007**, *17*, 2697–2702.

(16) Karaman, M. W.; Herrgard, S.; Treiber, D. K.; Gallant, P.; Atteridge, C. E.; Campbell, B. T.; Chan, K. W.; Ciceri, P.; Davis, M. I.; Edeen, P. T.; Faraoni, R.; Floyd, M.; Hunt, J. P.; Lockhart, D. J.; Milanov, Z. V.; Morrison, M. J.; Pallares, G.; Patel, H. K.; Pritchard, S.; Wodicka, L. M.; Zarrinkar, P. P. A quantitative analysis of kinase inhibitor selectivity. *Nature Biotechnol.* **2008**, *26*, 127–132.

(17) Carpinelli, P.; Ceruti, R.; Giorgini, M. L.; Cappella, P.; Gianellini, L.; Croci, V.; Degrossi, A.; Texido, G.; Rocchetti, M.; Vianello, P.; Rusconi, L.; Storici, P.; Zugnoni, P.; Arrigoni, C.; Soncini, C.; Alli, C.; Patton, V.; Marsiglio, A.; Ballinari, D.; Pesenti, E.; Fancelli, D.; Moll, J. PHA-739358, a potent inhibitor of Aurora kinases with a selective target inhibition profile relevant to cancer. *Mol. Cancer Ther.* **2007**, *6*, 3158–3168.

(18) Howard, S.; Berdini, V.; Boulstridge, J. A.; Carr, M. G.; Cross, D. M.; Curry, J.; Devine, L. A.; Early, T. R.; Fazal, L.; Gill, A. L.; Heathcote, M.; Maman, S.; Matthews, J. E.; McMenamin, R. L.; Navarro, E. F.; O'Brien, M. A.; O'Reilly, M.; Rees, D. C.; Reule, M.; Tisi, D.; Williams, G.; Vinkovic, M.; Wyatt, P. G. Fragment-based discovery of the pyrazol-4-yl urea (AT9283), a multitargeted kinase inhibitor with potent Aurora kinase activity. *J. Med. Chem.* **2009**, *52*, 379–388.

(19) Oslob, J. D.; Romanowski, M. J.; Allen, D. A.; Baskaran, S.; Bui, M.; Elling, R. A.; Flanagan, W. M.; Fung, A. D.; Hanan, E. J.; Harris, S.; Heumann, S. A.; Hoch, U.; Jacobs, J. W.; Lam, J.; Lawrence, C. E.; McDowell, R. S.; Nannini, M. A.; Shen, W.; Silverman, J. A.; Sopko, M. M.; Tangonan, B. T.; Teague, J.; Yoburn, J. C.; Yu, C. H.; Zhong, M.; Zimmerman, K. M.; O'Brien, T.; Lew, W. Discovery of a potent and selective Aurora kinase inhibitor. *Bioorg. Med. Chem. Lett.* **2008**, *18*, 4880–4884.

(20) Arbitrario, J. P.; Belmont, B. J.; Evanchik, M. J.; Flanagan, W. M.; Fucini, R. V.; Hansen, S. K.; Harris, S. O.; Hashash, A.; Hoch, U.; Hogan, J. N.; Howlett, A. R.; Jacobs, J. W.; Lam, J. W.; Ritchie, S. C.; Romanowski, M. J.; Silverman, J. A.; Stockett, D. E.; Teague, J. N.; Zimmerman, K. M.; Taverna, P. SNS-314, a pan-Aurora kinase inhibitor, shows potent anti-tumor activity and dosing flexibility in vivo. *Cancer Chemother. Pharmacol.* **2010**, *65*, 707–717.

(21) Adams, N. D.; Adams, J. L.; Burgess, J. L.; Chaudhari, A. M.; Copeland, R. A.; Donatelli, C. A.; Drewry, D. H.; Fisher, K. E.; Hamajima, T.; Hardwicke, M. A.; Huffman, W. F.; Koretke-Brown, K. K.; Lai, Z. V.; McDonald, O. B.; Nakamura, H.; Newlander, K. A.; Oleykowski, C. A.; Parrish, C. A.; Patrick, D. R.; Plant, R.; Sarpong, M. A.; Sasaki, K.; Schmidt, S. J.; Silva, D. J.; Sutton, D.; Tang, J.; Thompson, C. S.; Tummino, P. J.; Wang, J. C.; Xiang, H.; Yang, J.; Dhanak, D. Discovery of GSK1070916, a potent and selective inhibitor of Aurora B/C kinase. *J. Med. Chem.* **2010**, *53*, 3973–4001.

(22) Hardwicke, M. A.; Oleykowski, C. A.; Plant, R.; Wang, J.; Liao, Q.; Moss, K.; Newlander, K.; Adams, J. L.; Dhanak, D.; Yang, J.; Lai, Z.; Sutton, D.; Patrick, D. GSK1070916, a potent Aurora B/C kinase inhibitor with broad antitumor activity in tissue culture cells and human tumor xenograft models. *Mol. Cancer Ther.* **2009**, *8*, 1808–1817.

(23) Fletcher, G. C.; Broxk, R. D.; Denny, T. A.; Hembrough, T. A.; Plum, S. M.; Fogler, W. E.; Sidor, C. F.; Bray, M. R. ENMD-2076 is an

orally active kinase inhibitor with antiangiogenic and antiproliferative mechanisms of action. *Mol. Cancer Ther.* **2011**, *10*, 126–137.

(24) Wang, S.; Midgley, C. A.; Scaerou, F.; Grabarek, J. B.; Griffiths, G.; Jackson, W.; Kontopidis, G.; McClue, S. J.; McInnes, C.; Meades, C.; Mezna, M.; Plater, A.; Stuart, I.; Thomas, M. P.; Wood, G.; Clarke, R. G.; Blake, D. G.; Zheleva, D. I.; Lane, D. P.; Jackson, R. C.; Glover, D. M.; Fischer, P. M. Discovery of *N*-phenyl-4-(thiazol-5-yl)pyrimidin-2-amine Aurora kinase inhibitors. *J. Med. Chem.* **2010**, *53*, 4367–4378.

(25) Glaser, K. B.; Li, J.; Marcotte, P. A.; Magoc, T. J.; Guo, J.; Reuter, D. R.; Tapang, P.; Wei, R. Q.; Pease, L. J.; Bui, M. H.; Chen, Z.; Frey, R. R.; Johnson, E. F.; Osterling, D. J.; Olson, A. M.; Bouska, J. J.; Luo, Y.; Curtin, M. L.; Donawho, C. K.; Michaelides, M. R.; Tse, C.; Davidsen, S. K.; Albert, D. H. Preclinical characterization of ABT-348, a kinase inhibitor targeting the Aurora, vascular endothelial growth factor receptor/platelet-derived growth factor receptor, and Src kinase families. *J. Pharmacol. Exp. Ther.* **2012**, *343*, 617–627.

(26) McLaughlin, J.; Markovtsov, V.; Li, H.; Wong, S.; Gelman, M.; Zhu, Y.; Franci, C.; Lang, D. W.; Pali, E.; Lasaga, J.; Low, C.; Zhao, F.; Chang, B.; Gururaja, T. L.; Xu, W.; Baluom, M.; Sweeny, D.; Carroll, D.; Sran, A.; Thota, S.; Parmer, M.; Romane, A.; Clemens, G.; Grossbard, E.; Qu, K.; Jenkins, Y.; Kinoshita, T.; Taylor, V.; Holland, S. J.; Argade, A.; Singh, R.; Pine, P.; Payan, D. G.; Hitoshi, Y. Preclinical characterization of Aurora kinase inhibitor R763/AS703569 identified through an image-based phenotypic screen. *J. Cancer Res. Clin. Oncol.* **2010**, *136*, 99–113.

(27) Jani, J. P.; Arcari, J.; Bernardo, V.; Bhattacharya, S. K.; Briere, D.; Cohen, B. D.; Coleman, K.; Christensen, J. G.; Emerson, E. O.; Jakowski, A.; Hook, K.; Los, G.; Moyer, J. D.; Pruimboom-Brees, I.; Pustilnik, L.; Rossi, A. M.; Steyn, S. J.; Su, C.; Tsaparikos, K.; Wishka, D.; Yoon, K.; Jakubczak, J. L. PF-03814735, an orally bioavailable small molecule Aurora kinase inhibitor for cancer therapy. *Mol. Cancer Ther.* **2010**, *9*, 883–894.

(28) Shimomura, T.; Hasako, S.; Nakatsuru, Y.; Mita, T.; Ichikawa, K.; Koda, T.; Sakai, T.; Nambu, T.; Miyamoto, M.; Takahashi, I.; Miki, S.; Kawanishi, N.; Ohkubo, M.; Kotani, H.; Iwasawa, Y. MK-5108, a highly selective Aurora-A kinase inhibitor, shows antitumor activity alone and in combination with docetaxel. *Mol. Cancer Ther.* **2010**, *9*, 157–166.

(29) Manfredi, M. G.; Ecsedy, J. A.; Meetze, K. A.; Balani, S. K.; Burenkova, O.; Chen, W.; Galvin, K. M.; Hoar, K. M.; Huck, J. J.; LeRoy, P. J.; Ray, E. T.; Sells, T. B.; Stringer, B.; Stroud, S. G.; Vos, T. J.; Weatherhead, G. S.; Wysong, D. R.; Zhang, M.; Bolen, J. B.; Claiborne, C. F. Antitumor activity of MLN8054, an orally active small-molecule inhibitor of Aurora A kinase. *Proc. Natl. Acad. Sci. U. S. A.* **2007**, *104*, 4106–4111.

(30) Manfredi, M. G.; Ecsedy, J. A.; Chakravarty, A.; Silverman, L.; Zhang, M.; Hoar, K. M.; Stroud, S. G.; Chen, W.; Shinde, V.; Huck, J. J.; Wysong, D. R.; Janowick, D. A.; Hyer, M. L.; Leroy, P. J.; Gershman, R. E.; Silva, M. D.; Germanos, M. S.; Bolen, J. B.; Claiborne, C. F.; Sells, T. B. Characterization of Alisertib (MLN8237), an investigational small-molecule inhibitor of Aurora A kinase using novel in vivo pharmacodynamic assays. *Clin. Cancer Res.* **2011**, *17*, 7614–7624.

(31) Shah, N. P.; Kim, D. W.; Kantarjian, H.; Rousselot, P.; Llacer, P. E.; Enrico, A.; Vela-Ojeda, J.; Silver, R. T.; Khoury, H. J.; Muller, M. C.; Lambert, A.; Matloub, Y.; Hochhaus, A. Potent, transient inhibition of BCR-ABL with dasatinib 100 mg daily achieves rapid and durable cytogenetic responses and high transformation-free survival rates in chronic phase chronic myeloid leukemia patients with resistance, suboptimal response or intolerance to imatinib. *Haematologica* **2010**, *95*, 232–240.

(32) Hodous, B. L.; Geuns-Meyer, S. D.; Hughes, P. E.; Albrecht, B. K.; Bellon, S.; Bready, J.; Caenepeel, S.; Cee, V. J.; Chaffee, S. C.; Coxon, A.; Emery, M.; Fretland, J.; Gallant, P.; Gu, Y.; Hoffman, D.; Johnson, R. E.; Kendall, R.; Kim, J. L.; Long, A. M.; Morrison, M.; Olivieri, P. R.; Patel, V. F.; Polverino, A.; Rose, P.; Tempest, P.; Wang, L.; Whittington, D. A.; Zhao, H. Evolution of a highly selective and potent 2-(pyridin-2-yl)-1,3,5-triazine Tie-2 kinase inhibitor. *J. Med. Chem.* **2007**, *50*, 611–626.

- (33) DiMauro, E. F.; Newcomb, J.; Nunes, J. J.; Bemis, J. E.; Boucher, C.; Buchanan, J. L.; Buckner, W. H.; Cee, V. J.; Chai, L.; Deak, H. L.; Epstein, L. F.; Faust, T.; Gallant, P.; Geuns-Meyer, S. D.; Gore, A.; Gu, Y.; Henkle, B.; Hodous, B. L.; Hsieh, F.; Huang, X.; Kim, J. L.; Lee, J. H.; Martin, M. W.; Masse, C. E.; McGowan, D. C.; Metz, D.; Mohn, D.; Morgenstern, K. A.; Oliveira-dos-Santos, A.; Patel, V. F.; Powers, D.; Rose, P. E.; Schneider, S.; Tomlinson, S. A.; Tudor, Y. Y.; Turci, S. M.; Welcher, A. A.; White, R. D.; Zhao, H.; Zhu, L.; Zhu, X. Discovery of aminoquinazolines as potent, orally bioavailable inhibitors of Lck: synthesis, SAR, and in vivo anti-inflammatory activity. *J. Med. Chem.* **2006**, *49*, 5671–5686.
- (34) Cee, V. J.; Albrecht, B. K.; Geuns-Meyer, S.; Hughes, P.; Bellon, S.; Bready, J.; Caenepeel, S.; Chaffee, S. C.; Coxon, A.; Emery, M.; Fretland, J.; Gallant, P.; Gu, Y.; Hodous, B. L.; Hoffman, D.; Johnson, R. E.; Kendall, R.; Kim, J. L.; Long, A. M.; McGowan, D.; Morrison, M.; Olivieri, P. R.; Patel, V. F.; Polverino, A.; Powers, D.; Rose, P.; Wang, L.; Zhao, H. Alkynylpyrimidine amide derivatives as potent, selective, and orally active inhibitors of Tie-2 kinase. *J. Med. Chem.* **2007**, *50*, 627–640.
- (35) Nguyen, H. N.; Cee, V. J.; Deak, H. L.; Du, B.; Faber, K. P.; Gunaydin, H.; Hodous, B. L.; Hollis, S. L.; Krolkowski, P. H.; Olivieri, P. R.; Patel, V. F.; Romero, K.; Schenkel, L. B.; Geuns-Meyer, S. D. Synthesis of 4-substituted chlorophthalazines, dihydrobenzoozepinediones, 2-pyrazolylbenzoic acid, and 2-pyrazolylbenzohydrazide via 3-substituted 3-hydroxyisindolin-1-ones. *J. Org. Chem.* **2012**, *77*, 3887–3906.
- (36) Asselin, S. M.; Bio, M. M.; Langille, N. F.; Ngai, K. Y. Practical access to metallo thiophenes: regioselective synthesis of 2,4-disubstituted thiophenes. *Org. Process Res. Dev.* **2010**, *14*, 1427–1431.
- (37) (a) Bayliss, R.; Sardon, T.; Vernos, I.; Conti, E. Structural basis of Aurora-A activation by TPX2 at the mitotic spindle. *Mol. Cell* **2003**, *12*, 851–862. (b) Anderson, K.; Yang, J.; Koretke, K.; Nurse, K.; Calamari, A.; Kirkpatrick, R. B.; Patrick, D.; Silva, D.; Tummino, P. J.; Copeland, R. A.; Lai, Z. Binding of TPX2 to Aurora A alters substrate and inhibitor interactions. *Biochemistry* **2007**, *46*, 10287–10295.
- (38) Sessa, F.; Mapelli, M.; Ciferri, C.; Tarricone, C.; Areces, L. B.; Schneider, T. R.; Stukenberg, P. T.; Musacchio, A. Mechanism of Aurora B activation by INCENP and inhibition by hesperadin. *Mol. Cell* **2005**, *18*, 379–391.
- (39) Claiborne, C. F.; Manfredi, M. G. Case study of Aurora-A inhibitor MLN8054. In *Kinase Inhibitor Drugs*; Li, R., Stafford, J. A., Eds.; John Wiley & Sons: Hoboken, NJ, 2009; pp 333–350.
- (40) Stepan, A. F.; Kauffman, G. W.; Keefer, C. E.; Verhoest, P. R.; Edwards, M. Evaluating the differences in cycloalkyl ether metabolism using the design parameter “lipophilic metabolism efficiency” (LipMetE) and a matched molecular pairs analysis. *J. Med. Chem.* **2013**, *56*, 6985–6990.
- (41) Tamaki, A.; Ierano, C.; Szakacs, G.; Robey, R. W.; Bates, S. E. The controversial role of ABC transporters in clinical oncology. *Essays Biochem.* **2011**, *50*, 209–232.
- (42) Liu, X.; Wright, M.; Hop, C. E. Rational use of plasma protein and tissue binding data in drug design. *J. Med. Chem.* **2014**, *57*, 8238–8248.
- (43) Zhao, Y.; Jona, J.; Chow, D. T.; Rong, H.; Semin, D.; Xia, X.; Zanon, R.; Spancake, C.; Maliski, E. High-throughput logP measurement using parallel liquid chromatography/ultraviolet/mass spectrometry and sample-pooling. *Rapid Commun. Mass Spectrom.* **2002**, *16*, 1548–1555.
- (44) Tan, H.; Semin, D.; Wacker, M.; Cheetham, J. An automated screening assay for determination of aqueous equilibrium solubility enabling SPR study during drug lead optimization. *JALA* **2005**, *10*, 364–373.
- (45) The percentage of bone marrow cells with 4N DNA provides a lagging indicator of Aurora B inhibition. Cells with 4N DNA content comprise G1-phase cells that have exited mitosis without dividing as well as G2/M phase cells. After an AKI is washed out of cells, restoration of baseline p-HH3 levels in this group of 4N DNA cells occurs faster than normalization of the cell cycle phase distribution in bone marrow.
- (46) This data is summarized in the Supporting Information along with PD data showing insignificant inhibition by **14b** at doses of 30 mg/kg with plasma concentration $\sim 26 \mu\text{M}$ and by **23k** (15 mg/kg dose and $0.66 \mu\text{M}$ plasma concentration).
- (47) As an indication of its cellular p38 α inhibition, AMG 900 inhibited LPS-induced secretion of TNF α in THP-1 cells with an IC₅₀ of 840 nM.
- (48) Gao, F.; Johnson, D. L.; Ekins, S.; Janiszewski, J.; Kelly, K. G.; Meyer, R. D.; West, M. Optimizing higher throughput methods to assess drug–drug interactions for CYP1A2, CYP2C9, CYP2C19, CYP2D6, rCYP2D6, and CYP3A4 in vitro using a single point IC₅₀. *J. Biomol. Screening* **2002**, *7*, 373–382.
- (49) These serum shift studies were performed with 60 min preincubation of AMG 900 and serum before the addition of cells. Shifts in IC₅₀ were not consistently observed in pilot serum shift studies measuring p-HH3 suppression after one hour of incubation with phthalazine AKIs without this preincubation step.
- (50) (a) Gomez, V.; Sese, M.; Santamaria, A.; Martinez, J. D.; Castellanos, E.; Soler, M.; Thomson, T. M.; Paciucci, R. Regulation of Aurora B kinase by the lipid raft protein flotillin-1. *J. Biol. Chem.* **2010**, *285*, 20683–20690. (b) Nguyen, H. G.; Chinnappan, D.; Urano, T.; Ravid, K. Mechanism of Aurora-B degradation and its dependency on intact KEN and A-boxes: identification of an aneuploidy-promoting property. *Mol. Cell. Biol.* **2005**, *25*, 4977–4992.
- (51) Unpublished results cited in this work showed a more persistent suppression of p-HH3 inhibition in cells treated with **6** relative to **3b**-treated cells, with the latter restored to baseline levels in 2 h. Anderson, K.; Lai, Z.; McDonald, O. B.; Stuart, J. D.; Nartey, E. N.; Hardwicke, M. A.; Newlander, K.; Dhanak, D.; Adams, J.; Patrick, D.; Copeland, R. A.; Tummino, P. J.; Yang, J. Biochemical characterization of GSK1070916, a potent and selective inhibitor of Aurora B and Aurora C kinases with an extremely long residence time. *Biochem. J.* **2009**, *420*, 259–265.
- (52) Bush, T. L.; Payton, M.; Heller, S.; Chung, G.; Hanestad, K.; Rottman, J. B.; Loberg, R.; Friberg, G.; Kendall, R. L.; Saffran, D.; Radinsky, R. AMG 900, a small-molecule inhibitor of Aurora kinases, potentiates the activity of microtubule-targeting agents in human metastatic breast cancer models. *Mol. Cancer Ther.* **2013**, *12*, 2356–2366.
- (53) Paller, C. J.; Wissing, M. D.; Mendonca, J.; Sharma, A.; Kim, E.; Kim, H. S.; Kortenhorst, M. S.; Gerber, S.; Rosen, M.; Shaikh, F.; Zahurak, M. L.; Rudek, M. A.; Hammers, H.; Rudin, C. M.; Carducci, M. A.; Kachhap, S. K. Combining the pan-Aurora kinase inhibitor AMG 900 with histone deacetylase inhibitors enhances antitumor activity in prostate cancer. *Cancer Med.* **2014**, *3*, 1322–1335.
- (54) (a) Markman, B.; Mahadevan, D.; Hurvitz, S.; Kotasek, D.; Shaheen, M.; Carducci, M.; Goodman, O.; Jiang, X.; Chow, V.; Juan, G.; Friberg, G.; Gamelin, E.; Desai, J. 7LBA Phase 1 dose-expansion study of AMG 900, a pan-Aurora kinase inhibitor, in adult patients with advanced taxane-resistant solid tumors. 26th EORTC-NCI-AACR Symposium on Molecular Targets and Cancer Therapeutics, Barcelona, Spain, Nov 18–21, 2014. *Eur. J. Cancer* **2014**, *50* (Suppl6), 197–198. (b) Friberg, G.; Payton, M. Use of AMG 900 for the Treatment of Cancer. WO2013181462A1, Dec 5, 2013.
- (55) Juan, G.; Bush, T. L.; Ma, C.; Manoukian, R.; Chung, G.; Hawkins, J. M.; Zoog, S.; Kendall, R.; Radinsky, R.; Loberg, R.; Friberg, G.; Payton, M. AMG 900, a potent inhibitor of Aurora kinases causes pharmacodynamic changes in p-histone H3 immunoreactivity in human tumor xenografts and proliferating mouse tissues. *J. Transl. Med.* **2014**, *12*, 307.
- (56) Huang, L.; Berry, L.; Ganga, S.; Janosky, B.; Chen, A.; Roberts, J.; Colletti, A. E.; Lin, M. H. Relationship between passive permeability, efflux, and predictability of clearance from in vitro metabolic intrinsic clearance. *Drug Metab. Dispos.* **2010**, *38*, 223–231.
- (57) Berry, L. M.; Zhao, Z. An examination of IC₅₀ and IC₅₀-shift experiments in assessing time-dependent inhibition of CYP3A4, CYP2D6 and CYP2C9 in human liver microsomes. *Drug Metab. Lett.* **2008**, *2*, 51–59.